AGU ADVANCING EARTH AND SPACE SCIENCES

Earth's Future

Key Points:
- 60% of Arctic coastal infrastructure detected by satellites (1,495 km^2) is located in low-lying areas, prone to erosion and Sea-Level Rise (SLR)
- 18% of all coastal settlements will be exposed to coastal erosion by 2030 and 45% to SLR in 2100
- By 2100, 77% of coastal infrastructure will see ground temperature at 2 m shift from negative to positive, based on 2000–2019 trend

Pan-Arctic Assessment of Coastal Settlements and Infrastructure Vulnerable to Coastal Erosion, Sea-Level Rise, and Permafrost Thaw

Rodrigue Tanguy[1,2] , Annett Bartsch[1,2] , Ingmar Nitze[3] , Anna Irrgang[3] , Pia Petzold[3] , Barbara Widhalm[1,2] , Clemens von Baeckmann[1,2], Julia Boike[3,4] , Julia Martin[3] , Aleksandra Efimova[1] , Gonçalo Vieira[5] , Dustin Whalen[6] , Birgit Heim[3] , Mareike Wieczorek[3] , and Guido Grosse[3,7]

[1]b.geos GmbH, Korneuburg, Austria, [2]Austrian Polar Research Institute, Vienna, Austria, [3]Alfred Wegener Institute, Helmholtz Centre for Polar and Marine Research, Potsdam, Germany, [4]Department of Geography, Humboldt University, Berlin, Germany, [5]Centre of Geographical Studies, Associate Laboratory TERRA, Institute of Geography and Spatial Planning, University of Lisbon, Lisbon, Portugal, [6]Geological Survey of Canada, Natural Resources Canada, Dartmouth, NS, Canada, [7]University of Potsadam, Potsdam, Germany

Abstract This study assesses the vulnerability of Arctic coastal settlements and infrastructure to coastal erosion, Sea-Level Rise (SLR) and permafrost warming. For the first time, we characterize coastline retreat consistently along permafrost coastal settlements at the regional scale for the Northern Hemisphere. We provide a new method to automatically derive long-term coastline change rates for permafrost coasts. In addition, we identify the total number of coastal settlements and associated infrastructure that could be threatened by marine and terrestrial changes using remote sensing techniques. We extended the Arctic Coastal Infrastructure data set (SACHI) to include road types, airstrips, and artificial water reservoirs. The analysis of coastline, Ground Temperature (GT) and Active Layer Thickness (ALT) changes from 2000 to 2020, in addition with SLR projection, allowed to identify exposed settlements and infrastructure for 2030, 2050, and 2100. We validated the SACHI-v2, GT and ALT data sets through comparisons with in-situ data. 60% of the detected infrastructure is built on low-lying coast (<10 m a.s.l). The results show that in 2100, 45% of all coastal settlements will be affected by SLR and 21% by coastal erosion. On average, coastal permafrost GT is increasing by 0.8°C per decade, and ALT is increasing by 6 cm per decade. In 2100, GT will become positive at 77% of the built infrastructure area. Our results highlight the circumpolar and international amplitude of the problem and emphasize the need for immediate adaptation measures to current and future environmental changes to counteract a deterioration of living conditions and ensure infrastructure sustainability.

Plain Language Summary We examine the exposure of Arctic coastal infrastructure and settlements to coastal erosion, sea-level rise (SLR) and permafrost warming. Based on trend analyses from the years 2000 to 2020, we have identified areas that will be affected by 2030, 2050, and 2100. Our research finds that by 2100, 45% of permafrost coastal settlements will be affected by SLR, and 21% will face infrastructure damage due to coastal erosion. Permafrost is warming by 0.8°C per decade, and the soil surface layer thawing every summer is deepening, which will most likely affect the majority of existing coastal infrastructure due to reduced ground stability. This is the first study assessing coastal settlements around the Arctic at risk from coastal erosion, SLR and permafrost warming along permafrost coasts with a consistent observation method. We estimate that numerous coastal settlements and their infrastructure will be affected by changing environmental conditions by 2100. These findings highlight the urgent need for adaptation strategies to mitigate infrastructure damage and protect the living conditions in Arctic permafrost coastal areas.

1. Introduction

Due to the amplified warming of the Arctic, its oceanic and terrestrial environment are experiencing rapid changes. Models project a significant increase of these changes by 2100 (IPCC, 2023), impacting the Arctic biosphere. The Arctic Ocean sea-ice extent and thickness is already rapidly declining (Meredith et al., 2019; Stroeve & Notz, 2018). Since 1979, the duration of open-water conditions along the entire Arctic coastline has nearly doubled, with a notable expansion into fall (Barnhart et al., 2014). Further decline of the summer sea-ice

extent is projected to decrease by 12.6% per decade and the open-water season to lengthen from 63 to 90 days by 2100, increasing the exposure time of the Arctic coasts to the erosive force of water (Crawford et al., 2021, 2022; Overeem et al., 2011). Rising air temperature, increasing ground temperature, and higher precipitation levels are causing the degradation of terrestrial permafrost (Smith et al., 2022; Vasiliev et al., 2020). Temperature measurements from the Global Terrestrial Network for Permafrost indicate an increase in permafrost temperature of 0.39°C per decade in the Arctic continuous permafrost zone, as reported by Biskaborn et al. (2019). Based on the combination of modeling and satellite-derived observations, permafrost GT at 2 m depth has been increasing on average by about 1°C from 1997 to 2019, across the Northern Hemisphere (NH) (Bartsch et al., 2023). A continued pace of this warming will very likely result in large scale near-surface permafrost loss by 2100 (Guo et al., 2023). Permafrost warming contributes to the deepening of the active layer, enhancing thermokarst processes where ground-ice thawing generates lake and thaw-pond formation, lake drainage, ground subsidence and coastal erosion (Nitzbon et al., 2024; Smith et al., 2022).

At the interface between land and sea, the permafrost coastline, as well as coastal settlements, are subject to various pressures. Arctic permafrost coasts are among the fastest eroding coasts on Earth, with local erosion rates exceeding 40 m/yr (Malenfant et al., 2022; Obu et al., 2017). The average pan-Arctic coastal retreat rate was estimated to 0.5 m/yr by Lantuit et al. (2012) and is expected to double before the end of the century (Nielsen et al., 2022). Erosion is a natural process but was observed to already accelerate in various regions during the last decades (Irrgang et al., 2018; Isaev et al., 2019; Jones et al., 2018; Tanguy, Whalen, Prates, Pina, et al., 2023; Tanguy, Whalen, Prates, & Vieira, 2023; Whalen et al., 2022). High retreat rates are mainly occurring where unconsolidated but ice-bound tundra cliffs are exposed to waves during the sea-ice free season and along low-lying areas prone to recurring flooding events (Obu et al., 2017). The Beaufort Sea coast is experiencing the highest mean retreat rates with 1.1 m/yr (Cunliffe et al., 2019; Overduin et al., 2014; Thomas et al., 2020).

The Global Mean Sea-Level (GMSL) has risen at a rate of 3.3 mm per year since 1993, with an acceleration observed during the twentieth century, mainly due to the loss of land ice and the thermal expansion of seawater (Cazenave et al., 2018; Frederikse et al., 2020). Due to multiple contributing factors, regional variability is significant and regional relative sea-level change needs to be considered when assessing potential impacts on coasts. The primary obstacle in studying Arctic sea-level variation is the lack of observational data. The majority of tide gauges with extensive sea-level records are located along the coast of Norway and Russia, with only a fraction of them being maintained after 1990. In the latest IPCC report on sea-level change, it is projected with medium confidence that most coastal areas will see a regional SLR that is within ±20% of the GMSL change (IPCC, 2023). However, in polar regions, uncertainty in future sea-level projections is influenced by the gravitational effects of ice-sheet melt. When large ice sheets, such as those in Greenland or Antarctica, melt, the reduction in gravitational pull causes local sea levels to drop, even as global sea levels rise (Kurtze, 2022). Additionally, post-glacial rebound can further decrease local sea levels like along the coasts of the Canadian Arctic Archipelago, Hudson Bay, Greenland, Svalbard, and northern Scandinavia (Boisson & Allard, 2020). Ocean reanalysis such as the ORAS5 model integrates available observational data with numerical modeling. According to the ORAS5 data for the 1978–2018 period, positive sea-level trends show an amplification in almost all basins within the Arctic Ocean. The Beaufort Sea shows the highest rates up to 9 mm/yr (1978–2018), and up to 15.9 mm/yr for the 1995–2018 period, with these patterns mainly driven by the intensification of the Beaufort Gyre system, and water salinity change from river and glacier freshwater inputs (Jin et al., 2023; Tajouri et al., 2024).

In the Arctic, strong cyclones predominantly occur in the Barents, Kara, Laptev, and Chukchi Seas, with projections suggesting they will intensify during summer as the climate warms (Atkinson, 2005; Day & Hodges, 2018). Observations over recent decades indicate that Arctic cyclones are becoming stronger and longer-lasting, particularly in the Barents, Kara, and Laptev Sea, (Zhang et al., 2023). This increase in storm activity leads to severe storm surges that pose significant threats to low-lying coastal settlements, such as those in northern Alaska (Henke et al., 2024). Several coastal communities, including Shishmaref in Alaska and Tuktoyaktuk in Canada, have been repeatedly impacted by coastal erosion, storm surges, and flooding (Marino & Lazrus, 2015; Whalen et al., 2022). It is important to note that high Arctic coasts, such as Longyearbyen in Svalbard, are significantly affected by coastal hazards. Additionally, glacier dynamics play a major role in driving landscape and environmental changes in this region (Jaskólski et al., 2018). These conditions present economic and environmental challenges for the stability of roads, airstrips, buildings, oil tanks, and pipelines, posing significant

engineering challenges for coastal infrastructure in the arctic (Buzard et al., 2021; Hjort et al., 2022; Streletskiy et al., 2019; Tanguy, Whalen, Prates, Pina, et al., 2023; Tanguy, Whalen, Prates, & Vieira, 2023).

Monitoring of Arctic coastlines and erosion has mostly been facilitated in the past at selected key sites by field studies and for selected coastal segments using high resolution aerial and satellite image analysis (Gibbs et al., 2021; Irrgang et al., 2018; Tanguy, Whalen, Prates, Pina, et al., 2023; Tanguy, Whalen, Prates, & Vieira, 2023). However, satellite data can potentially be used to implement a circum-Arctic monitoring scheme for coastline changes, thereby overcoming the limitations of spatially selective monitoring. This specifically also includes the location of settlements and infrastructure and the quantification of coastal erosion rates (Bartsch et al., 2021; Irrgang et al., 2019). Core challenges include the size of the region to be covered and the needed spatial detail.

The Sentinel-1/2 derived Arctic Coastal Human Impact data set (SACHI-v1; Bartsch et al., 2021) shows increasing human presence and industrial activity linked to oil/gas exploitation and mining within the arctic coastal zone. This data set considered three types of human impact as visible from space: linear transport infrastructure (roads and railways), buildings and other constructions (e.g., bridges), and other impacted areas (gravel pads, open pit mining areas, etc.) and was limited to a 100 km fringe from the Arctic and permafrost coastline. In that classification, for example, airstrips were not distinguished individually and were included in the "other impacted area" class, and different road construction types (gravel vs. tarmac) were not considered. Initial analyses showed the potential of satellite data to separate road types (Bartsch, Ley, et al., 2020; Bartsch, Pointner, et al., 2020). Artificial water bodies were also not included, although water surfaces can be easily detected with satellite data. These features are built for water supply or sewage treatment near settlements but also by the oil and mining industry for industrial water usage, where they potentially could also cause accumulations of contaminants and local pollution (Glotov et al., 2018). The classification of different types of road, airstrips and the addition of water reservoirs substantially enhances the characterization of human impact zones and risk assessments including the socio-economic values of the various infrastructure.

Permafrost coastline evolution is commonly assessed using historical aerial photography combined with high-resolution satellite imagery, or airborne data (Irrgang et al., 2022). The variety of scales, investigated time periods and study sites make it difficult to compare observed changes between regions and to get a comprehensive picture of pan-Arctic coastal dynamics. The Arctic Coastal Dynamic Database (ACD) from Lantuit et al. (2012) provided a first compilation of shoreline change data, filling observational gaps with expert estimates. Landsat satellite imagery is a valuable data source due to its free availability, and large spatio-temporal coverage. Widely used for land-cover change studies, it can also be used to assess coastline evolution. However, the 30 m spatial resolution limits the detection of small changes (Xu, 2018). The study of Nitze et al. (2017) provided an efficient machine-learning based method using Landsat-trends to detect lake dynamics based on a probability measure for land to water and water to land conversion. Bartsch, Ley, et al. (2020), Bartsch, Pointner, et al. (2020) demonstrate the utility of an adaptation of this approach for Arctic coastline change identification.

In this study, we use satellite-derived coastal erosion rates in combination with SLR projections, permafrost changes, and a new classification of infrastructure types to reveal the impact of environmental changes on Arctic permafrost coastal settlements. We (a) provide a revised and updated version of the SACHI-v1 pan-Arctic infrastructure data set, incorporating new classifications including road types, airstrips, and artificial water reservoirs; (b) estimate coastal dynamics and erosion rates along areas with coastal settlements, using Landsat-based land-cover change detection based on the approach of Bartsch, Ley, et al. (2020), Bartsch, Pointner, et al. (2020); and (c) identify coastal settlements and infrastructure potentially exposed to coastal erosion, SLR, ground temperature, and active layer thickness changes over short-, mid-, and long-term time-scales (2030, 2050, 2100). All generated data sets were thoroughly validated and assessed for accuracy.

2. Study Area

Our analysis is covering the coast bordering the Arctic Ocean. In addition, we extended our study area to the south, to include the majority of NH permafrost-dominated coastlines. The infrastructure analysis considers a similar extent to the SACHI-v1 data set, defined as a 100 km buffer along Arctic and permafrost-dominated coasts, allowing to include settlements located within estuaries and deltas. The SACHI data set extends from northwest

Figure 1. Coastal settlements are shown, distinguishing between permanently inhabited settlements and the "Other" category, which includes infrastructures related to mining, the gas/oil industry, military stations, or abandoned sites. The SACHI 100 km coastal zone (black; Bartsch et al., 2021) and the extent of coastal dynamics derived from Landsat (purple) are shown. Permafrost zones are based on Obu et al. (2021c). Coastline types were simplified based on data from various sources: Alaska (deposit type; Jorgenson et al., 2008), Canada (Geological class; Robertson, 2015), Russia (FAO soil types; Stolbovoi & McCallum, 2002), and Greenland/Svalbard (backshore form; Lantuit et al., 2012). Validation sites and detailed information are provided in the supporting file.

Alaska through the northern coast of the American continent including the Canadian Arctic Archipelago to the Hudson Bay until Newfoundland. Greenland, Svalbard and East Scandinavia are included as well as the entire Russian coast (Figure 1). This area represents 62,000 km^2 and includes a total of 447 settlements, with 318 being directly located at the coast as identified in (Bartsch et al., 2021). These settlements are defined as areas with concentrated infrastructure, like hamlets, towns, mining or military bases, however some of them may not be permanently inhabited and are associated with industrial infrastructures of military station, sometimes abandoned. According to Ramage et al. (2021), the total coastal population living in permafrost regions is reported to be 1.1 million in 2017. Out of this total, 113,000 individuals reside on continuous permafrost, which is the primary focus of this study.

The extent of the coastline dynamics data set is more restricted due to the lack of sufficient Landsat acquisitions for the time series analysis and due to the frequent presence of sea-ice along very-high latitude coasts (e.g., Canadian Archipelago), making the data set less accurate in some regions (e.g., Iceland, Scandinavia, northern parts of the Canadian Arctic Archipelago). The Hudson Bay region was excluded from the analysis due to its strong post-glacial uplift (Andrews, 1970), and the Newfoundland region due to its dominantly rocky coastline (Figure 1).

3. Data

3.1. Infrastructure Data Set: Sentinel-1/2

Similarly to the first version of the SACHI data set, this work uses a combination of Sentinel-1 (Synthetic Aperture Radar; SAR) and Sentinel-2 (multi-spectral optical) for the detection of human infrastructure footprints along Arctic and permafrost-dominated coasts (Bartsch et al., 2024). In total, 484 Sentinel-2 granules at 100 by 100 km extent were acquired from 2016 to 2020. More details on data and framework are described in Bartsch, Ley, et al. (2020), Bartsch, Pointner, et al. (2020) and Bartsch et al. (2021).

3.2. Coastline Dynamics Data Set: Landsat

Coastline change areas were retrieved using satellite data from Landsat 5, 7 and 8 from the Thematic Mapper (TM), Enhanced Thematic Mapper Plus (ETM+) and Operational Land Image sensors, also covering NH permafrost-dominated coasts. The scenes were acquired between 2000 and 2020 in order to represent recent coastal changes, also due to sparse data acquisition before 2000 in Siberia and Northern Alaska. Some areas were excluded from the analysis due to tiles with sparse temporal coverage or quality issues due to frequent cloud cover or sea-ice presence even in summer. We applied a filtering of images available between July and August with cloud cover below 70%. The used Landsat bands have a spatial resolution of 30 m: Blue, Green, Red, Near-Infrared (NIR), Shortwave Infrared 1 (SWIR1), and Shortwave Infrared 2 (SWIR2).

3.3. Coastal Elevation and Regional Sea-Level Change

The elevation was extracted for each infrastructure element from a new coastal digital terrain model (deltaDTM; (Pronk, 2024)), which provides a bias corrected version of the Copernicus digital elevation model (ESA, 2023). The product was compared to high resolution data and reveals an overall error of less than 1 m (Pronk et al., 2024). In addition, data from the IPCC AR6 regional sea-level change projection was used to estimate low-lying infrastructure at risk from SLR by the year 2100 (Fox-Kemper et al., 2021; Garner et al., 2022; Kopp et al., 2023; Slangen et al., 2023). The projection models are based on the 1995–2014 time-period and integrate tide-gauge measurements for available stations. In the AR6 sea-level projections, significant improvements were made over AR5, incorporating higher-resolution ocean and ice-sheet models, resulting in more accurate regional predictions. However, uncertainties in regional SLR remain significant, especially in the Arctic, due to complex factors such as ice-sheet instability, ocean circulation changes, and vertical land movement. In the Arctic, subsidence caused by permafrost degradation and glacial isostatic adjustment complicates accurate regional sea-level projections. Furthermore, the lack of local data, due to the limited distribution of tide gauges and GNSS stations, contributes significantly to the uncertainties in future scenarios of regional sea-level change in the Arctic basin. Under the SSP2-4.5 scenario, regional SLR projections for the Arctic are generally expected to be in the range of 0.3–0.8 m by 2100 (IPCC, 2023; Masson-Delmotte et al., 2021; Slangen et al., 2023).

3.4. Permafrost Ground Temperature and Active Layer Thickness

Permafrost, while not directly observable from space, can be indirectly modeled through satellite data, for example, through observations of land surface temperatures essential for modeling GT and ALT. We used time series data from 1997 to 2019, leveraging a combination of satellite-derived land-surface temperatures (MODIS) and reanalysis data (ERA5 near-surface air temperature) (Obu et al., 2021a, 2021b; Westermann, Langer, et al., 2015; Westermann, Østby, et al., 2015), from the European Space Agency's Climate Change Initiative Permafrost project (ESA Permafrost_cci). This modeling, at roughly 1 km resolution, helps to identify permafrost change trends, particularly noted for increasing temperatures in the Northern Hemisphere, with significant changes along coastal regions facing high erosion rates (Bartsch et al., 2023; Bartsch, Ley, et al., 2020; Bartsch, Pointner, et al., 2020; Miner et al., 2022). Annual change trends for GT and ALT were calculated for the period 2000–2019. This data set was previously combined with the SACHI-v1 data set from Bartsch et al. (2021). Comprehensive validation information is available within the documentation (Heim et al., 2021) but it has not been specifically assessed along Arctic coastlines. Uncertainties for ALT were found to be higher than for GT and therefore a dedicated evaluation of ALT was carried out.

3.5. Validation Data

In-situ and very-high resolution (VHR) data were used to validate infrastructure coastline change rates and permafrost properties (GT at 2 m and ALT, CALM et al., 2024; Martin et al., 2023) at various sites. The supporting information file provides detailed information on validation data, location, and procedure (refer to Table S1 in the Supporting Information S2).

4. Methods

4.1. General Approach

This work provides an update to the previously published Sentinel-1/2 derived Arctic Coastal Human Impact data set (SACHI), incorporating new classes such as asphalt, gravel, and undefined roads, airstrips, and artificial water reservoirs. Areas of coastal erosion and accretion were derived from Landsat change probabilities for the period 2000–2020. Coastline change rates were retrieved and combined with the infrastructure data set in order to evaluate settlements exposure to coastal erosion for short-, mid-, and long-term scenarios (2030, 2050, and 2100, respectively). To identify coastal infrastructure and settlements exposed to erosion, future coastline positions for 2030, 2050, and 2100 were extrapolated using historical erosion rates derived from Landsat pixel-based analysis. Although the Bruun Rule could be used to estimate future coastline positions by integrating SLR, this method was not applied due to its high uncertainty. Additionally, the use of deltaDTM, which provides only low to medium spatial resolution for coastal topography, further limits its applicability. Moreover, the Bruun Rule is not well-suited for large-scale circumpolar studies, where coastal dynamics are highly complex and variable (Cooper & Pilkey, 2004).

Additionally, GT and ALT trends were considered in the evaluation of permafrost thaw exposure. The SACHI-v2 took into account settlements and infrastructure within the 100 km buffer zone of the coastline, as well as for the GT and ALT analysis. The analysis extent was restrained to a 1 km fringe from the coast for exposure analysis. Low-lying infrastructure (<10 m) was considered for estimating where settlements potentially will be affected by future SLR until 2100. New settlements and associated information were added to the settlement database. The fusion of coastline change rates, regional SLR, and changes in permafrost properties with the infrastructure data set allowed for the identification of settlements impacted by 2100. The overall workflow is shown in Figure 2. Sea-ice conditions play a critical role in reducing coastal erosion in the Arctic by protecting shorelines from wave action, particularly during storms. However, this parameter was not considered in this work since it is a secondary factor explaining coastal erosion. This study focus on primary factors such as long-term coastal erosion and permafrost trends (GT and ALT) and SLR, over a period of 20 years, which have direct impact on infrastructure durability.

4.2. Update of SACHI Infrastructure Data Set

The scheme uses Deep Learning (DL) techniques, in particular a U-Net convolutional neural network architecture using the deep learning framework Keras, and pixel-based Machine Learning, in particular Gradient Boosting Machines (GBM). The DL component uses Sentinel-2 and the GBM component Sentinel-1 and -2. The satellite data and retrieval scheme used in this study is described in Bartsch, Ley, et al. (2020) and Bartsch et al. (2021). In both cases, DL and GBM, super-resolution processing was applied to the 20 m bands of Sentinel-2 in order to obtain a 10 m nominal resolution data set for all used bands as input. Atmospheric correction from Sen2Cor processor was applied.

In our study, the DL component has been extended through the inclusion of additional classes consisting of three road types (asphalt, gravel and undefined) and airstrips/airports. The calibration data set for all classes has been revised in order to account for inaccuracies in the OpenStreetMap data set which was used initially. A k-means post-processing on road features (using the Sentinel-1/2 bands) was applied to evaluate the possibility to distinguish gravel from asphalt roads. The GBM component provided a water class using a pixel based approach. Results for the water class have been separated and added to the database when in proximity to settlements. These water bodies were manually revised and only artificial water bodies (e.g., reservoirs) within settlements were kept. This typically includes rectangular or circle-like objects, as well as lakes enclosed by open pit mining activities.
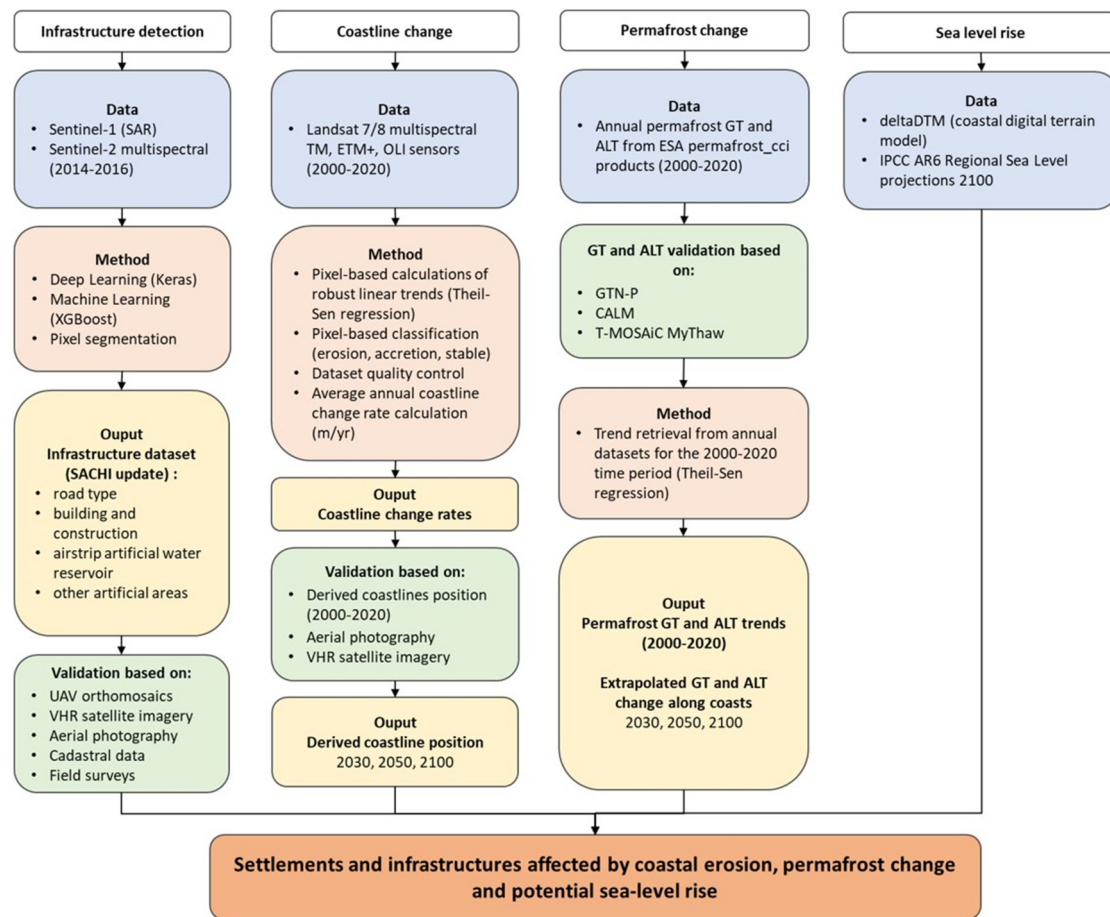
Figure 2. Detailed analysis workflow. SAR: Synthetic Aperture Radar; XGBoost: eXtreme Gradient Boosting; CALM: Circumpolar Active Layer Monitoring; T-MOSAiC: Terrestrial Multidisciplinary distributed Observatories for the Study of Arctic Connections.

4.3. Permafrost Coastline Dynamics Retrieval

Following the approach of Nitze et al. (2017), the Landsat time-series were used for pixel-level calculations of probabilities of erosion and accretion (change from land to water and vice versa) as well as no change, for the time period 2000 to 2020. A threshold for separation of change areas was determined in Bartsch, Ley, et al. (2020), as a 50% probability value was found applicable and has been also applied in the present study for the classification of changes. The resulting raster information was converted to vector polygons. To facilitate circumpolar implementation, several post-processing steps have been introduced. The Landsat results were limited within a 1 km buffer along the coast in order to limit further analyses to coastline related changes, while still considering lagoons, deltas and estuaries. Manual quality control was performed to detect and remove misclassification errors induced by coastal lake change, snow, sea-ice, land-fast ice, tidal changes and infrastructure removal/construction (examples shown in Figure 3).

4.3.1. Coastline Change Rate Calculation

A common approach to determine the rate of shoreline change is to use the Digital Shoreline Analysis System (DSAS) developed by USGS, which uses time series of vector shoreline positions to calculate rate-of-change statistics at regular spaced perpendicular transects along a coast (Thieler et al., 2009). This method is effective when using manually delineated coastlines, but is not suitable for large automatically extracted data sets. In our case, the nature of the polygonal geometry of the derived change areas allows for a simplified estimation of the average rate of coastline change derived for each polygon. These polygons are in general elongated features, parallel to the coastline. The polygon length and area were calculated. The mean width (average coastline change) was calculated assuming an idealized rectangular representation of the change area, from which annual rates of
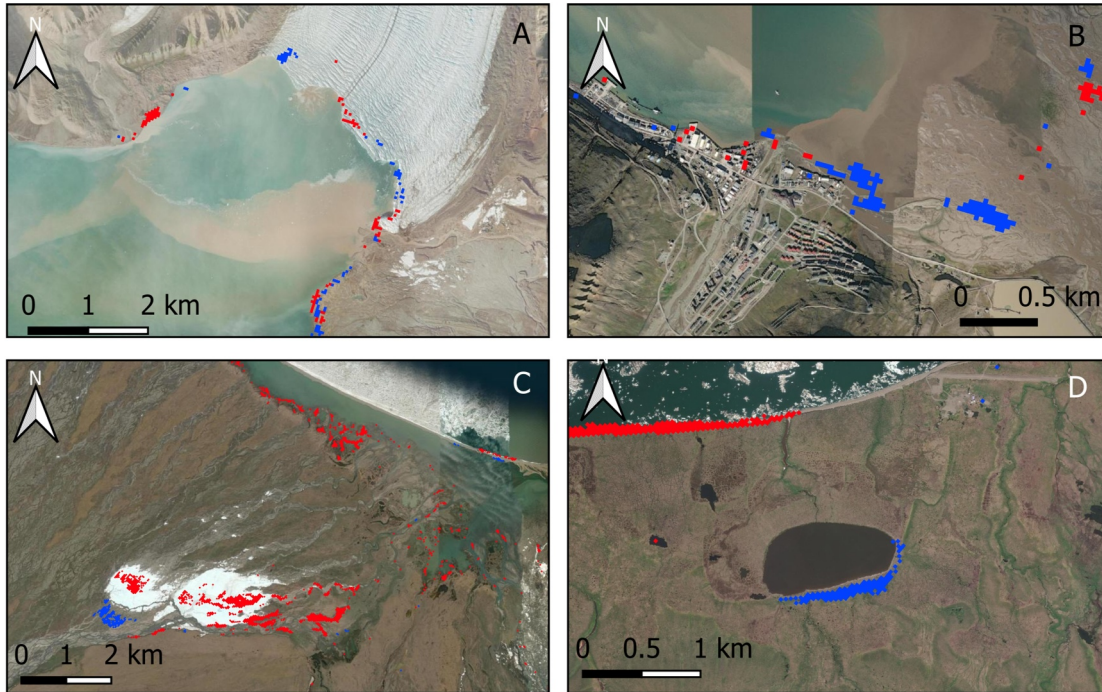
Figure 3. Examples of classification errors as seen with the polygons outside the coastal zone in the raw data set and needing manual checking and removal. These errors can be induced by glaciers and sea-ice (a), infrastructure (b), snow, and deltas (c), or lake changes (d). The blue polygons show accretion and the red erosion. Background map: Esri©, USGS.

change were subsequently calculated (Figure 4). To evaluate the accuracy of this method, we also applied the DSAS workflow to the polygons in test areas by converting the polygons to lines and splitting the shape into a seaward side and a landward side line, corresponding to the 2000 and 2020 coastline in the case of erosion, and vice versa for accretion. This strategy requires additional manual editing of the polygons and was also applied to validate the overall quality of the Landsat probabilities, extending the validation of the coastline position in Bartsch, Ley, et al. (2020) to more sites.

4.3.2. Coastline Change Rate Uncertainty

Calculating the uncertainty associated to coastline position is necessary in order to evaluate the reliability of the coastline change rates (Del Río & Gracia, 2013). The Equation 1 provides the coastline change rate uncertainty (U) which was calculated using the coastline position uncertainty (U_{CP}) for each coastline, divided by the number of years of the analyzed time period (t).

$$U = \sqrt{(U_{CP1}^2 + U_{CP2}^2)/(t_2 - t_1)} \tag{1}$$

Figure 4. Implementation of the automatic method to calculate the annual change rate of a detected change area. The area is divided by the length to obtain a mean width, which is eventually divided by the length of the observation period (t, in years).

Table 1
Feature Count and Total Area in the Updated Infrastructure Data Set - SACHI-v2 (100 km Coastal Zone)

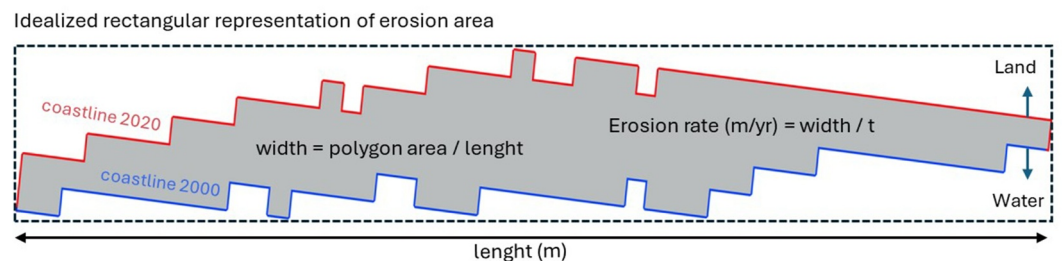| Class		SACHI-v1		SACHI-v2	
		Feature count	Area (km^2)	Feature count	Area (km^2)
Roads	Asphalt	428,872	643	289,631	130
	Gravel			533,317	300
	Undefined			247,455	170
Buildings and other constructions		219,052	199	208,947	125
Other artificial areas	Airstrips	264,732	371	2,149	6
	Artificial water reservoirs			6,914	134
	Undefined artificial areas			222,407	629
Total		912,656	1,213	1,510,820	1,495

The coastline position uncertainty is incorporating the image pixel resolution (m) and the georeferencing error, RMSE (m). The polygons which were retrieved from the Landsat change detection analyses show changes which occurred within a 20-year time-span (2000–2020). The landward and seaward polygon boundaries were defined as the respective coastlines for the year 2000 and 2020. The uncertainty was also calculated for the coastline derived from validation data (Table 2).

4.4. Ground Temperature and Active Layer Thickness Validation

Permafrost_cci products for GT and ALT were validated in Heim et al. (2021). Additional validation was done for the ALT using new in-situ thaw-depth measurements (T-MOSAiC, Boike et al., 2021; CALM et al., 2024; Martin et al., 2023). The data and procedure are described in the Supporting Information S1. GT and ALT for 2019 and trends were extracted from the permafrost_cci products (Obu et al., 2021a, 2021b) at infrastructure extent as well as for the entire study extent. Linear trend extrapolation for 2030, 2050, and 2100 was applied to understand the distribution and magnitude of potential change in future decades.

4.5. Settlements Exposed to Sea-Level Rise

The mean elevation at infrastructure footprints was extracted from the deltaDTM (Pronk et al., 2024). To assess potential exposure to SLR by 2100, regional SLR projections were applied to low-lying coastal infrastructure, using median change values for the medium confidence scenario SSP2-4.5, which corresponds to intermediate greenhouse gas emissions and a projected global temperature increase of 2.7°C by 2100 (Wang et al., 2018). Infrastructure was considered at risk if, after subtracting the projected SLR (extrapolated inland), the elevation fell below 0.75 m. This threshold accounts for the root-mean-square error (RMSE) of the deltaDTM. While this approach identifies infrastructure potentially at risk from SLR, it does not accurately distinguish between permanent or temporary flooding risks.

5. Results

5.1. Infrastructure Mapping

5.1.1. Updated SACHI Data Set

In total, we mapped an infrastructure footprint of 1495 km^2 in the SACHI-v2 (considering the same extent as the first version), resulting in an increase by 282 km^2, or 19%, by adding previously unmapped infrastructure (Table 1). Artificial water reservoirs account for 6914 supplementary features (134 km^2) and roads have been subclassified into three different types. Gravel roads represent 50% of the total detected roads and asphalt roads 22%, with the remaining being classified as undefined roads. In total, 448 settlements centers were identified within the full data set extent (100 km buffer from coastline). We account for 318 settlements located directly at the coast (<1 km). These settlements specifically represent an infrastructure area of 468 km^2. The majority are traditional living communities which maintain longstanding practices such as fishing, hunting, and herding activity (53%). Industrial settlements for mining activity or gas/oil extraction represent 20% while the remaining settlements
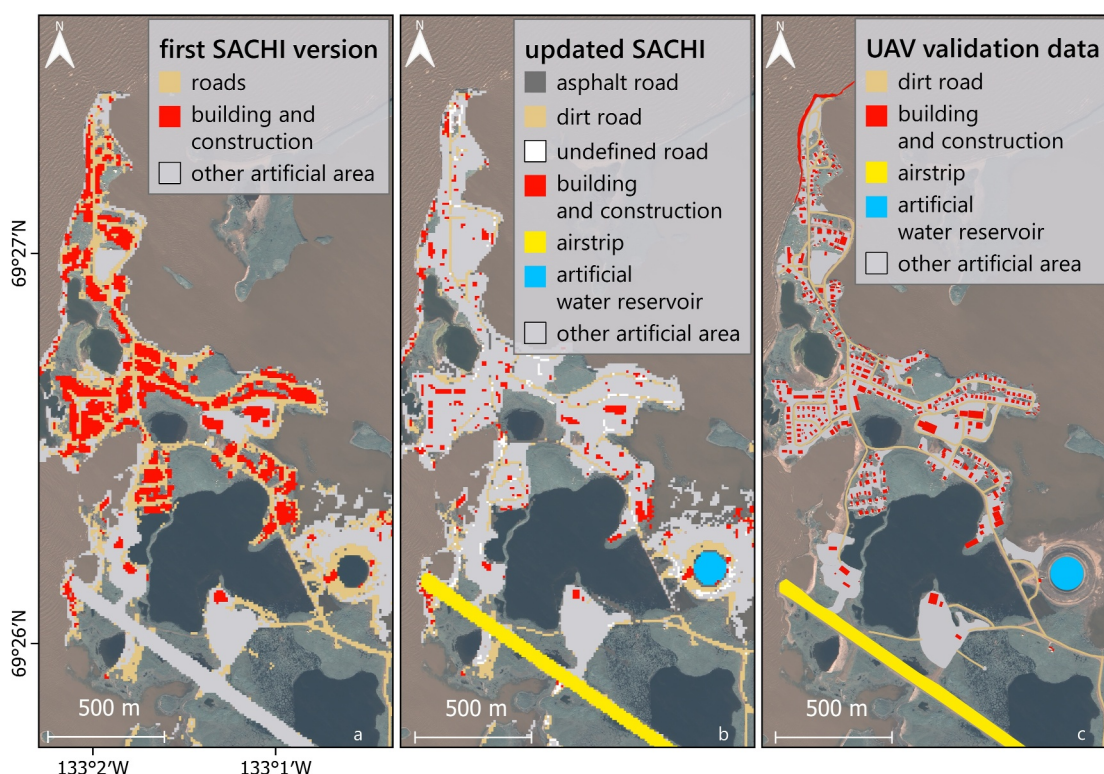
Figure 5. Examples of SACHI versions: (a) SACHI-v1 (Bartsch et al., 2021), (b) updated SACHI-v2, and (c) validation data from the 2019 UAV orthomosaic at the Hamlet of Tuktoyaktuk (Canadian Beaufort coast). Background map: Pléiades©; CNES, 2018, Airbus DS.

represent other uses such as tourism or military facilities and research or weather stations (based on settlement center data as in Bartsch et al. (2021)). According to (Ramage et al., 2021), the population of inhabitants in coastal settlements within our study area is 162,000.

5.1.2. SACHI-v2 Accuracy Assessment

The data set accuracy was evaluated with validation data provided from VHR imagery and map data sets (<1 m), including UAV, satellite and aerial imagery, and cadastral data over several settlements (Table S1 in the Supporting Information S2). The agreement with the 10 m based classification result is 67% with the best detection of 80% for airstrips and other artificial areas such as bare-ground patches, gravel pads, open pit and mining areas (Table S2 in the Supporting Information S2). Roads show an overall accuracy of 58% and the post-processing results for road types reveal a good accuracy for the detection of asphalt roads (76%), but only around 40% on average for gravel roads. Buildings are accurately detected in 57% and the minimum detectable building size is 100 m^2, as determined by UAV surveys in the hamlets of Paulatuk and Tuktoyaktuk in NW Canada. The SACHI-v1 overestimated the extent of buildings and other constructions. This issue is evident in the Hamlet of Tuktoyaktuk in Northwest Canada (Figure 5). The SACHI-v2 shows significant improvements in the mapping of airstrips, buildings and other constructions and is better able to distinguish individual objects.

Comparison of road objects with an in situ road survey in Svalbard (2021) revealed good detection of roads below 10 m width. In fact, in SACHI-v2 we were able to detect roads with widths from 2.7 to 12 m. For the road type survey (asphalt and gravel) in Longyearbyen, Svalbard, 75% were represented in the data set showing a mean width of 5.7 m. However, only 34% were correctly classified. Among these, 40% asphalt roads were correctly classified with mean width of 6.3 m, and up to 21% of the gravel roads showing a mean width of 4.9 m. 25% of the roads found in the survey were not detected in the data set.

Table 2
Inter-Comparison Between Rate Calculation Methods for Validation and Landsat Derived Data Using the Digital Shoreline Analysis System Workflow and the Polygon Geometry Method for Change Rate Calculations

		Barter island	Mackenzie delta front	Newtok	Point lonely air field
Validation Data	Represented period	2000–2020	2000–2018	2005–2019	2000–2018
	DSAS mean change rate (m/yr)	−3.01	−4	−12.9	−15.8
	Uncertainty (m/yr)	±0.26	±0.14	±0.36	±0.28
Landsat derived data 2000–2020	Polygons mean change rate (m/yr)	−3.36	−3.54	−9.2	−7.9
	DSAS mean change rate (m/yr)	−3.63	−4.1	−9.5	−8.02
	Uncertainty (m/yr)	±2	±2	±2	±2
Difference	Validation - Landsat Polygon rates (m/yr)	0.35	−0.46	−3.7	−7.9
	Validation - Landsat DSAS rates (m/yr)	0.62	0.1	−3.4	−7.78
	Landsat Polygon - Landsat DSAS rates (m/yr)	0.27	0.56	0.3	0.12

Note. See Table S2 in the Supporting Information S2 for characteristics and uncertainty levels associated to the data.

5.2. Coastline Changes and Exposed Settlements

5.2.1. Coastline Changes Accuracy Assessment

The uncertainty in the coastline change rate derived from Landsat data is approximately 2 m/yr, as detailed in Table 2. The results reveal that on the four validation sites, the coastline change rates between validation and Landsat-derived rates can differ from −7.9 to 0.35 m/yr, where positive values represent an overestimation of erosion from the Landsat data and where negative values represent an underestimation of erosion. The comparison between calculated rates with the DSAS extension and the polygon approach shows a very good fit along the coasts of Barter Island and the Mackenzie Delta front. At Point Lonely and Newtok (Alaska), the Landsat polygon approach shows an underestimation of the erosion rate.

Point Lonely Air Field, 190 km east of Prudhoe Bay, experiences some of the highest erosion rates in the region, up to 19 m/yr. This significant erosion primarily affects the tundra cliffs, characterized by ice-wedge polygons and block failures along the bluffs (Figure 6). Regarding the validation rates from DSAS, the first period (2000–2009) is characterized by a mean coastline retreat rate of 8.3 m/yr, while the second period (2009–2018) is characterized by an acceleration of the erosion reaching 23.5 m/yr. The coastline is eroding at the average pace of 15.8 m/yr during the period 2000–2020. The Landsat results show a lower rate (−7.9 ± 2 m/yr). The Landsat analysis captured the bluff-top erosion clearly but indicates a gap in capturing the retreat of the lagoon's barrier beach. The narrowness of the beach (Figure 6), possibly exacerbated during storms, might have rendered it undetectable. Furthermore, the turbidity of the lagoon waters could have affected the accuracy of the Landsat pixel classification, complicating the differentiation between the lagoon and the open ocean.

At Newtok, the Landsat analysis is underestimating the validation rates by 3.7 m/yr over the period 2005–2019. The retreat has been poorly captured along the mudflat area fronting the settlement eastwards (Figure 7b). Moreover, the validation data was acquired for a shorter time-period than the Landsat data (see Table S1 in the Supporting Information S2).

An additional comparison was made between the Landsat rates using the simplified polygon rate retrieval and the DSAS method. The results show that the automatic method for rate calculation for the Landsat polygons is very accurate and shows an overall underestimation of 0.3 m/yr compared to the DSAS transect based method (last row of Table 2). Regarding the validation rates, the Landsat polygon rates tend to underestimate the coastline change rates, however, Figures 6 and 7 show examples of an overall good estimation of the coastlines evolution.

5.2.2. Settlements and Infrastructure Exposed to Coastal Erosion

Over the time period 2000–2020, significant coastline position changes were investigated close to 318 settlements located directly at the coast. These changes represent a total of 476 km of coastline length, showing an average change rate of −0.8 m/yr. Erosion is the dominant process, affecting 70% of the investigated coast. Maximum
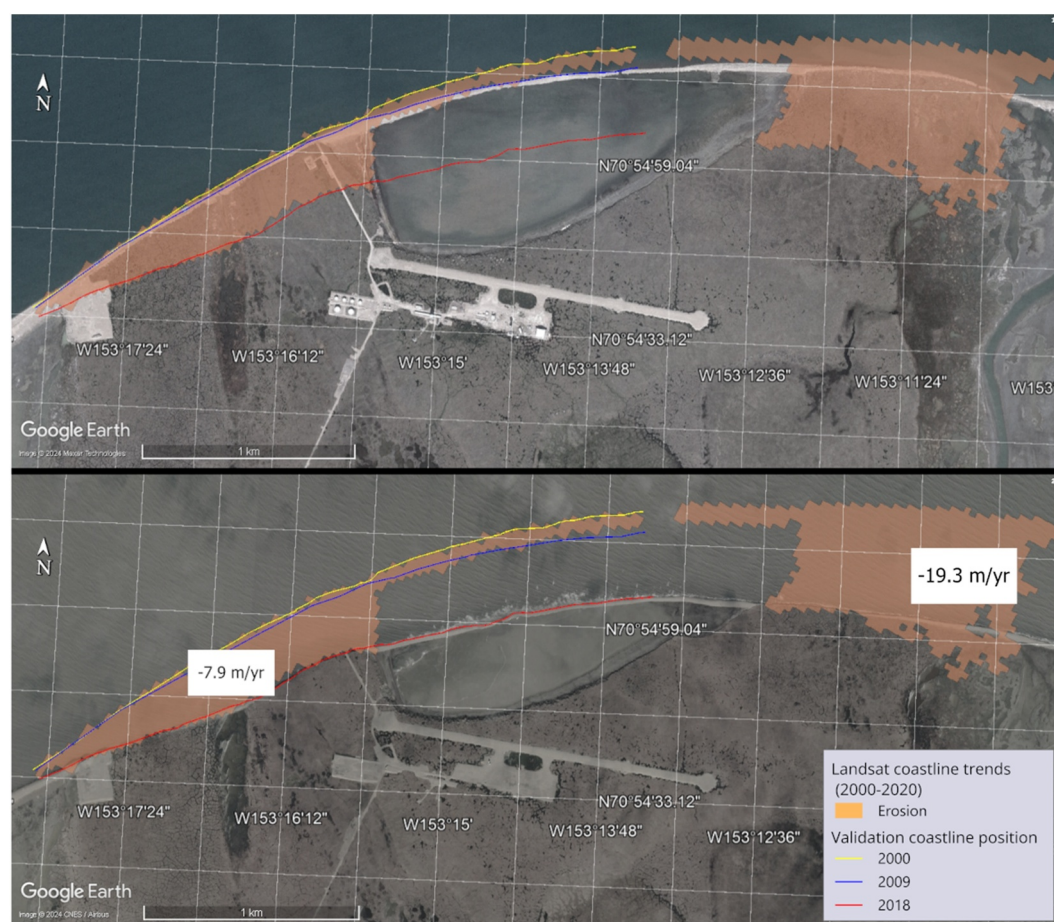
Figure 6. High erosion and infrastructure loss at Point Lonely Air Field. The scenes are from July 2009 and 2018. The orange overlapping area represents erosion area retrieved from Landsat trends. We note a very good fit with the shorelines of 2000 and 2018 along the bluff, however the barrier beach migration was not well captured. The coastline positions were derived from very-high resolution satellite imagery corresponding to Ikonos©-2000 (0.8 m spatial resolution); WorldView-1-2009 (0.5 m) and Pléiades© CNES/Airbus-2018 (0.5 m). Background map: Google Earth, ©2009, 2018, Maxar Technologies.

erosion rates of 20.4 m/yr were found near the Point Lonely Air Field. Accretion is located along highly dynamic coastal forms such as barrier islands, beaches and spits, with maximum rates close to 13 m/yr (Table 3).

Over the entire study area, the linear extrapolation of coastline positions for 2030, 2050, and 2100, reveals that 18% of the coastal settlements will be subject to infrastructure damage or loss due to coastline retreat in 2030 and 2050 and up to 21% in 2100. Along these specific settlements, the average erosion rate is about −3.2 m/yr. The difference is due to the fact, that some settlements are built a bit more inland and will only get affected later. Given a linear extrapolation of rates, by 2100 the total surface area of infrastructure and artificial areas (as detected with the 10 m resolution) potentially at risk by coastal erosion equals to 22 km^2, representing nearly 8% of the total low-lying coastal infrastructure area (see Figure A3). These settlements are mainly associated with residential areas with traditional food-harvesting activities (45%) and 33% with gas/oil and mining industry. Other affected settlements are already abandoned or are military or weather stations. As seen in the Figures A2 and A3, the Alaskan coast stands out, with 25 settlements exposed to coastal erosion by 2100. We account for 34 exposed settlements along the Russian coasts by 2100, mainly located along the Chukchi Peninsula (12), and Central North Siberian coast (20, Laptev and Kara Sea). In Svalbard, the settlements of Longyearbyen, Barentsburg, and Svea are predicted to be affected by coastal erosion by 2030. In Canada and within our analysis extent, only 2 settlements are expected to be exposed to erosion by 2100, Tuktoyaktuk (NWT), and Kugluktuk (Nunavut). Note that Tuktoyaktuk infrastructure is already significantly affected by coastal erosion.
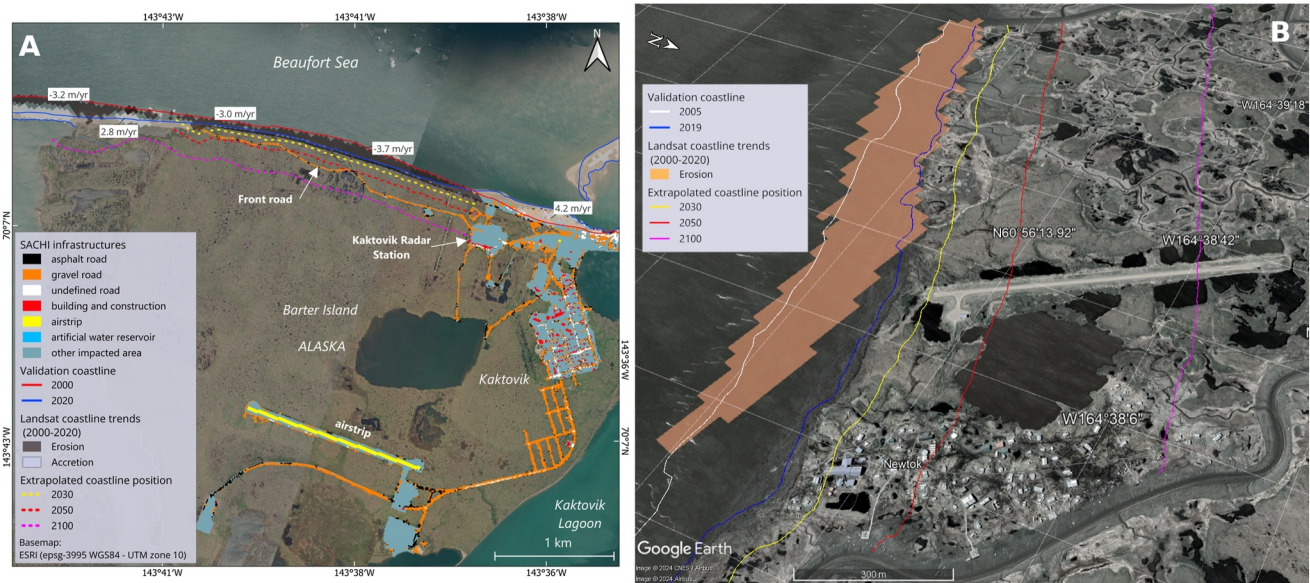
Figure 7. Example of results with merged infrastructure and coastline dynamics data sets, showing potential loss of infrastructures at Kaktovik and at Newtok. At Barter Island (a), the front road and the radar station may be affected in the long-term. At Newtok, coastal erosion averaging 9.2 m/yr has already destroyed infrastructures. In case erosion continues at such a great pace, the majority of the settlement is expected to disappear by 2100 (purple line). The coastline positions were derived from very-high resolution satellite imagery corresponding to Ikonos©-2005 (0.8 m spatial resolution) and Pléiades©CNES/Airbus-2019 (0.5 m). Maps Data: (a) ESRI; (b) GoogleEarth, CNES/Airbus, 2022.

Figure 7 shows the future coastline positions and potential infrastructure loss at Kaktovik (U.S. Beaufort Sea) and Newtok (U.S. Bering Sea). The erosion rates have been accurately detected at these settlements although being too conservative. The northern coast of Barter Island is exposed to erosion rates of 3.4 m/yr in front of the bluff-top. Accretion is present along spits and along a 600 m long section of the frontal beach of the island, fronting the settlement. This section shows an accretion rate of 4.2 m/yr. The coastline position estimated for 2100 shows a potential loss of infrastructure due to coastal erosion, such as the front road of the island and a part of the radar station of Kaktovik (Figure 7a).

Newtok is also an example of high erosion rates, where it would cause a loss of the majority of the infrastructure if no relocation plan is implemented. This is evident in the projected coastline positions for the mid- and long-term (Figure 7b). The projected coastline positions may underestimate areas at risk (from the airstrip toward the east) as seen with the difference between the red overlapping area and the validation coastlines. Although our projections are conservative, they do show the loss of critical infrastructure over the mid- and long term periods.

5.3. Regional Sea-Level Change and Exposed Settlements

Regarding the IPCC projections by 2100 for the SSP2-4.5 scenario, Arctic sea-level is expected to change from −2 to +0.98 m within the Arctic region (Garner et al., 2022; IPCC, 2023). High increase is localized south of the Barents Sea, in the Laptev Sea (Lena Delta region), and especially along the Beaufort Sea coast (+0.73–+1.26 m

Table 3
Coastline Dynamics at Settlement Vicinity for the Period 2000–2020

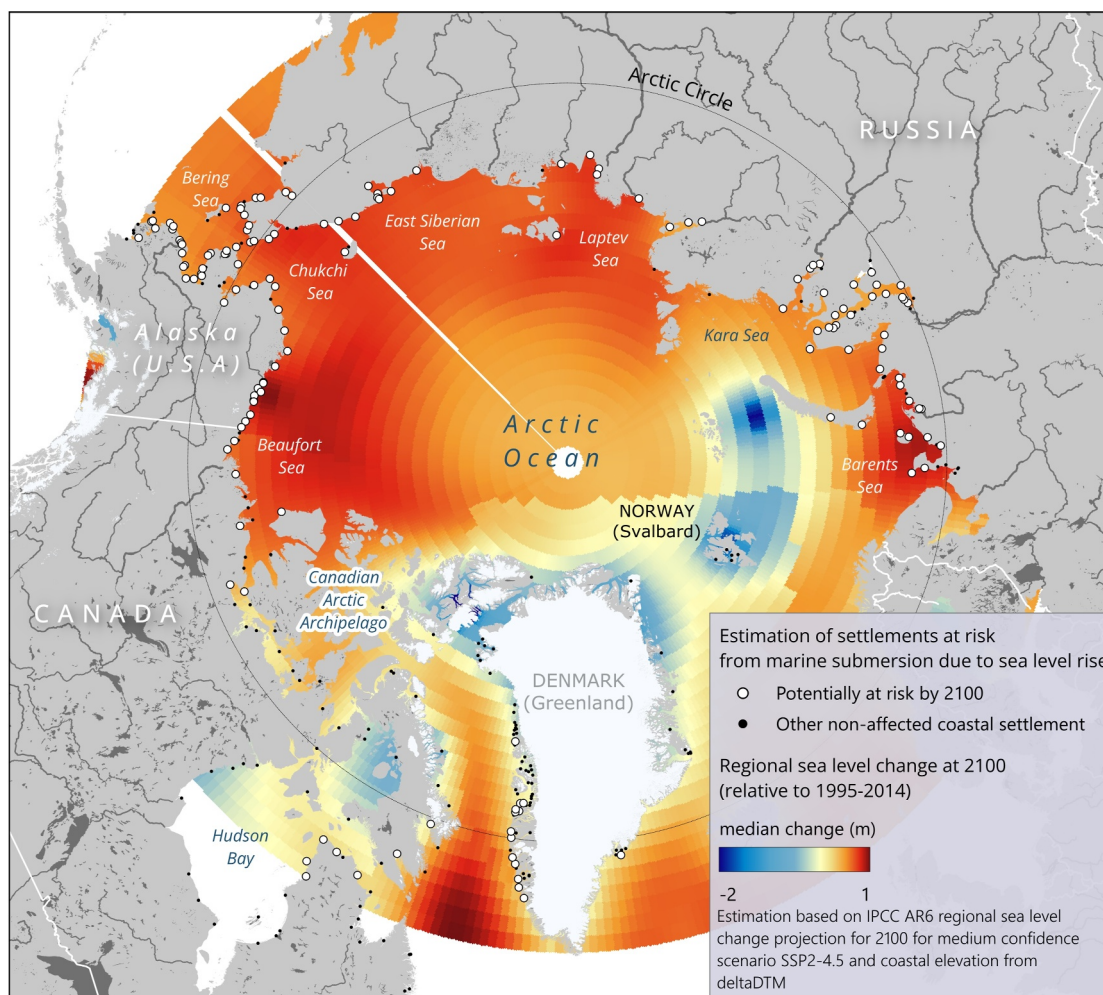|	No of settlement	Mean change rate (m/yr)	Erosion			Accretion		
			Mean rate (m/yr)	Max. Rate (m/yr)	Length (km)	Mean rate (m/yr)	Max. Rate (m/yr)	Length (km)
Total coastal settlements	318	−0.8	−2.9	−20.4	336	3.2	12.7	140
Settlements impacted in 2100	68	−1.8	−3.2	−20.4	150	2.9	4.5	20

Figure 8. Settlements potentially exposed to marine submersion in 2100. The estimation is based on IPCC AR6 regional sea-level projection for 2100 at medium confidence scenario SSP2-4.5 (Garner et al., 2022).

in 2100). Due to isostatic uplifting processes, some regions, such as northern Greenland and Canadian Arctic Archipelago and Svalbard, are experiencing negative sea-level change (Figure 8). From the coastal infrastructure within 1 km from the coast, 60% are located in low-lying areas (<10 m). According to our study area, SLR by 2100 could potentially submerge 6% of the low-lying infrastructure, which amounts to 18 km^2. This represents 45% of the total coastal settlements (318), as detailed in Figure 8 and the Figure A3 We found that 4% of the infrastructure exposed to erosion by 2100 will also be affected by SLR. This accounts for 51% of the settlements vulnerable to coastal erosion, primarily located along the Alaskan and Russian coasts. In Canada, all settlements exposed to coastal erosion are also exposed to SLR, by 2100 (Figure A3). Note that these results should be interpreted with caution due to the uncertainty in both the elevation model (deltaDTM) and the regional SLR projections for 2100.

5.4. Potential Permafrost Thaw and Infrastructure

5.4.1. Active Layer Thickness Accuracy Assessment

The comparison between T-MOSAiC, CALM observational network, and Permafrost_cci ALT data sets within a 10 km radius is detailed in Figure S2, spanning various study sites. In summary, the comparison emphasizes the difficulty in accurately capturing spatial variability in ALT in the Permafrost_cci product due to site-specific factors and limitations in model resolution, leading to discrepancies between modeled and measured values
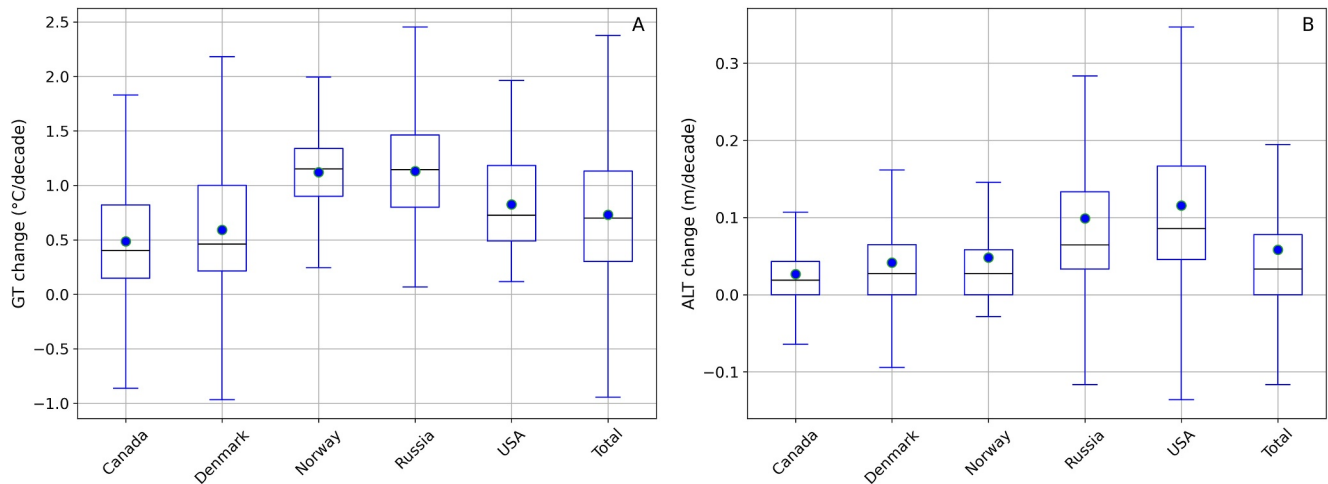
Figure 9. Decadal trends along permafrost-dominated coasts separated by regions for (a) Ground temperature (GT) at 2 m depth and (b) Active layer thickness (ALT). The extent is shown in Figure 9. Trends were derived from Permafrost_cci data (Obu et al., 2021a, 2021b). Outliers have been removed.

across various locations, but in particular where landscape heterogeneity is high. The comparison between the T-MOSAiC 2021 myThaw data set and the Permafrost_cci ALT data set is outlined in Figure S4. The agreement between the Permafrost_cci ALT and the measured ALT data was satisfactory for certain stations: Samoylov in Siberia, Russia; Toolik Lake in Alaska, USA; and the Zackenberg "wet" transect in Greenland. However, there were notable differences observed for several sites: both Bayelva transects in Svalbard, Norway; Kevo Vaisejaeggi in Finland; Siksik Creek in Trail Valley Creek, Canada; Cambridge Bay in Canada; and the Zackenberg "dry" transect in Greenland. These discrepancies can be attributed to the nature of the T-MOSAiC measurements, which are conducted throughout the entire summer, as opposed to the Permafrost_cci ALT, which represents the end-of-season values. Consequently, the seasonal evolution of the ALT is not adequately captured by the modeled data set, leading to inconsistencies in certain locations. The comparison between T-MOSAiC and Permafrost_cci ALT data sets highlights significant spatial variability challenges, particularly evident at T-MOSAiC sites in Svalbard and Zackenberg. Despite their proximity (about 500 m), the two T-MOSAiC sites in Svalbard exhibited notably different median ALT values (1.2 and 0.8 m), which were better represented within the Permafrost_cci ALT data set within a 10 km radius. This discrepancy underscores the challenge of reproducing diverse ALT values due to site-specific factors like soil properties, snow cover, vegetation height, and water level, which are not adequately captured by the model's coarse spatial resolution (0.926 km). Similar results were observed at the Zackenberg transects, where the T-MOSAiC ALT measured at the "dry" transect extended beyond those at the "wet" transect and the Permafrost_cci ALT data set. At the Kevo Vaisejaeggi and Siksik Creek sites, the Permafrost_cci ALT values were at least twice as high as the measured values, indicating discrepancies between the modeled and measured data. Conversely, at Cambridge Bay, the measured ALT was almost three times the modeled ALT, highlighting further inconsistencies between the data sets. Overall, the comparisons highlight variability in ALT measurements across different data sets and sites, underscoring the importance of considering various local factors such as soil type, ice content, snow and vegetation cover. Absolute ALT values from Permafrost_cci therefore need to be treated with care.

5.4.2. Coastal Permafrost Conditions

The calculated trends from the Permafrost_cci time-series shows increasing GT and ALT in the study area since the last 20 years. The GT have increased by 0.8°C/decade on average with maximum values near 3°C/decade, while ALT has increased by 6 cm/decade on average with maximum increase up to 2 m/decade (Figures 9 and 10). The Russian and Svalbard coasts show the highest average increase of GT (+1.1°C/decade). Highest average ALT increase is found along the Russian coast and Alaskan coasts (almost 10 cm/decade).
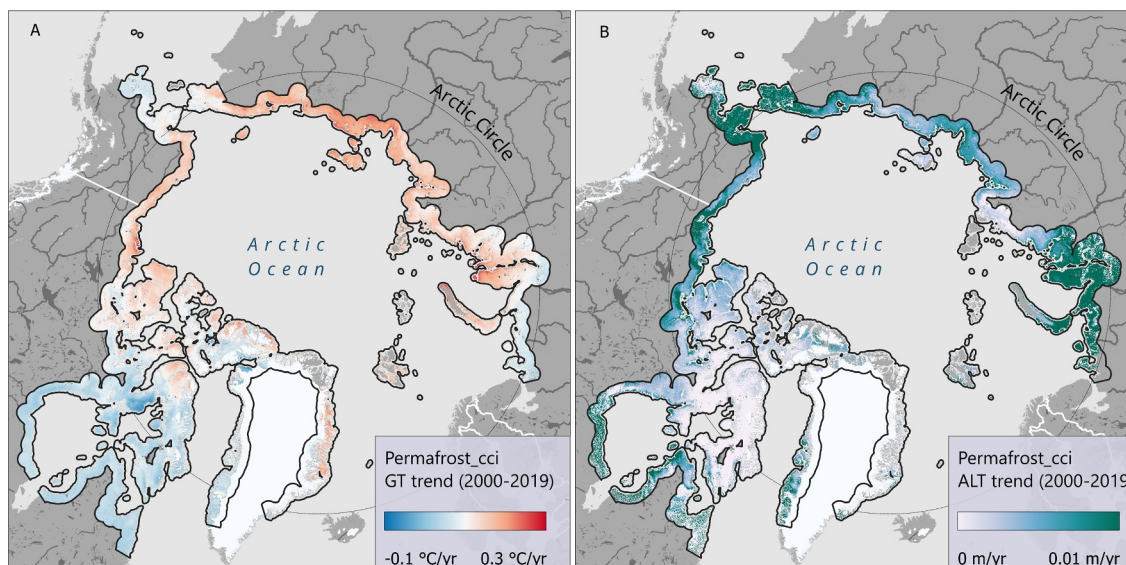
Figure 10. Trends for Ground Temperature at 2 m depth (a) and Active Layer Thickness (b) based on the 2000–2019 period, at study extent. Trends were derived from Permafrost_cci data (Obu et al., 2021a, 2021b).

5.4.3. Infrastructure and Changing Permafrost Conditions

Of the coastal infrastructure area, 45% is built on ground experiencing warming from 1 to 2°C/decade and 85% in areas with ALT increasing from 0 to 4 cm/decade (Figure 11). In 2019, the average GT was −2.3°C and ALT less than 1 m deep in our mapped infrastructure extent for all regions. 83% of the coastal infrastructures are built above ground with negative temperature (at 2 m depth), experiencing increasing GT. Based on trends, extrapolated GT and ALT at infrastructure areas for 2030, 2050, and 2100 show a strong increase for all countries. By 2100, 77% of the coastal infrastructure will experience a shift from negative to positive GT, with expected average temperature of 4–5°C by 2100 (in the mapped coastal infrastructure extent), which could strongly trigger ground subsidence. Svalbard, Russia, and Alaska are expected to experience shifting ground temperature toward positive values by 2050 reaching values above 6°C in 2100 (Figure 12a). The ALT in our mapped infrastructure extent is expected to increase significantly in the next decades, especially for Russia and Alaska for which the ALT could double by 2050, reaching up to 2 m in 2100 (Figure 12b). Canada shows the lowest average ALT in 2019, due to the high northern location of settlements. Changing permafrost conditions in the coastal area could induce thaw subsidence, and further degrade the stability of buildings and infrastructure (Figure 11).

6. Discussion

6.1. Infrastructure Identification

This study focuses on analyzing settlements and infrastructure in coastal areas dominated by permafrost. The new SACHI-v2 data set provides improved information on infrastructure occurrence in the Arctic, particularly for roads, airstrips and other artificial areas. Due to the limitation to 10 m nominal resolution, 33% of human related features were not captured across the validation sites. Specifically, road and building detection is challenging. The amount of detectable buildings is controlled by the resolution and the quality of the Sentinel-1 (radar) and Sentinel-2 data (multi-spectral), which limit the detection of small constructions, and object misclassification can occur with the presence of snow patches, rock outcrops, landfills, construction debris and large driftwood accumulations along the shore. Asphalt roads are scarcely present in the Arctic and along permafrost coasts, since the majority of roads are made of gravel, which is easier and cheaper to construct and maintain. In some settlements, roads are made of concrete blocks, falling in the undefined category. Although the Sentinel-2 imagery has been processed for atmospheric corrections (aerosol optical thickness and water vapor), clouds are still influencing the data quality and can lead to misclassification in addition to calibration and training data issues. The DL and GBM algorithms were trained on specific areas, however, the terrain heterogeneity across the Arctic
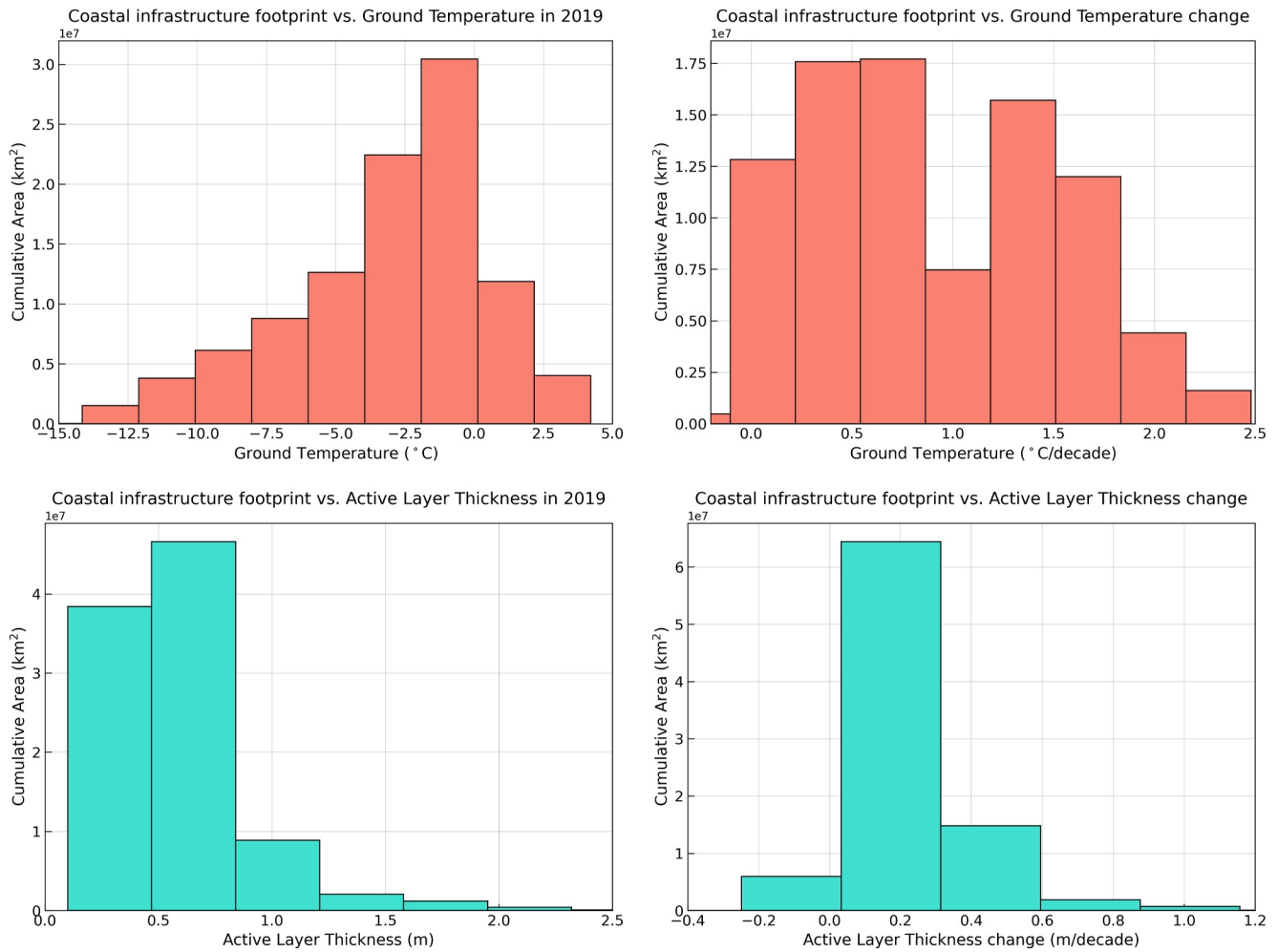
Figure 11. Distribution of GT and ALT for 2019 and annual change rate at the extent of coastal infrastructures. The change rates were calculated over the 2000–2019 period. Trends were derived from Permafrost_cci data (Obu et al., 2021a, 2021b).
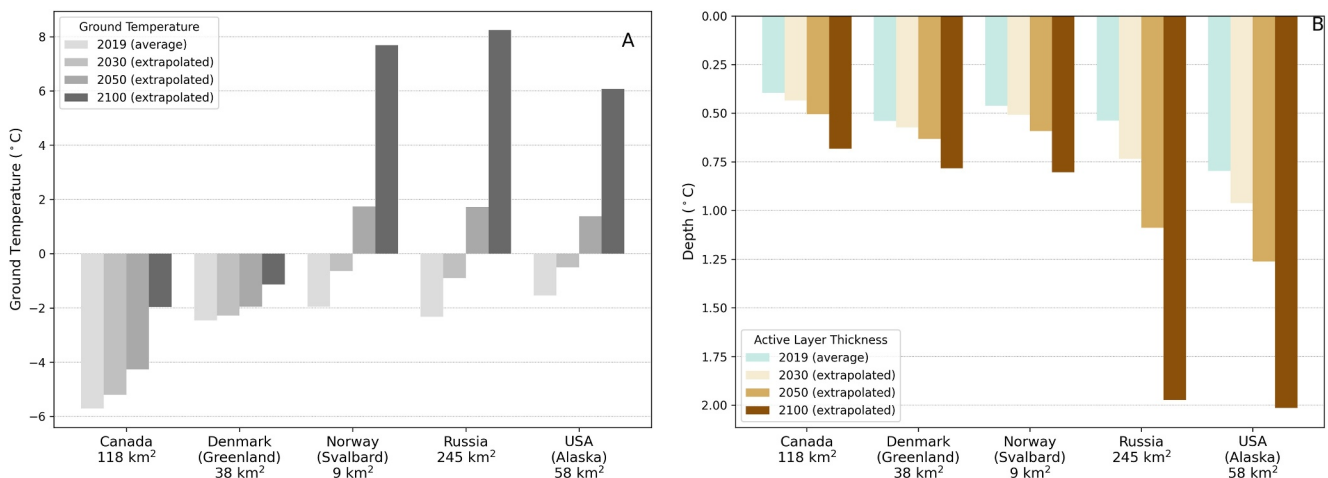
Figure 12. Average and extrapolated GT (a) and ALT (b), for different time-period at the mapped coastal infrastructure extent, based on the rates for the 2000–2019 period. GT and ALT trends were derived from Permafrost_cci data (Obu et al., 2021a, 2021b).

and along permafrost coasts influences the performance of the algorithms. It could be shown that Sentinel-1/2 data allow capturing also roads below 10 m width in some cases. Individual building detection needs to be improved with DL and GBM using VHR optical images. However, their processing remains challenging at regional scale. The Sentinel-1 SAR (Synthetic Aperture Radar) images were used for the GBM processing. Polarization, incidence angle effects inherent to SAR images may affect image quality and result in detection issues of spatial features (Kumar, 2021). Moreover, air and ground temperature and wetness are critical parameters influencing back-scatter values (Bergstedt et al., 2018). Nevertheless, the assessment shows that the 10 m spatial resolution allows consistent identification of human impacted areas such as very small settlements with few houses, which need to be considered in risk assessment studies across the entire Arctic. However, our results remain conservative in the estimation of total building area.

6.2. Coastline Changes

The use of consistent Landsat time-series for the detection of coastline changes within a period of 20 years shows to be efficient to provide estimations of average coastline rates on a regional to pan-Arctic scale. Although the results agree with validation data, it is crucial to emphasize that our methodology only detects rapid coastline changes that exceed 2 m per year. Changes falling below this threshold could not be considered in the trend analysis. Therefore, the approach may underestimate average coastline change rates, since smaller changes were not detected. However, for various reasons, the results can also underestimate the amount of infrastructure potentially exposed. Some sites in Alaska known for significant erosion, such as Utqiagvik or Kivalina, were not detected. One reason could be that more complex coastal settings with for example, highly dynamic barrier islands or frequent ice cover also in summer are still difficult to properly detect with the automated coastline extraction using the 20-year Landsat trends. According to the results, erosion is generally dominating along the studied settlements located on unconsolidated permafrost coasts. Some permafrost coasts can also show large accretion rates, localized along beaches and spits. Both erosion of the bluff-top and such processes can occur simultaneously along the same coastline segments (Tanguy, Whalen, Prates, Pina, et al., 2023; Tanguy, Whalen, Prates, & Vieira, 2023).

Moreover, local and regional studies based on the analysis of VHR imagery, revealed accelerating erosion in recent years in various areas of the Arctic (Hansen et al., 2015; Tanguy, Whalen, Prates, Pina, et al., 2023; Tanguy, Whalen, Prates, & Vieira, 2023) revealing a potentially further growing economic risks (Ogorodov et al., 2020). This acceleration is currently not considered in the analyses of rates and future impacts due to the need for higher spatial resolution in order to separate sub-periods and our simplified assumption of linear continuation of erosion rates into the future.

The assessment of coastline changes at the regional scale, as well as the detection of inter-annual variability of coastline changes, remains a challenge when using open-access satellite data. Compared to transect-based analyses (DSAS), our study estimates only average rates within changing areas, and does not consider regular transects spacing such as in the DSAS framework. Moreover, a shoreline reference is not consistently defined with this method. In fact, the Landsat trends detect change from water to land and land to water and do not consistently allow distinguishing between the retreat of a bluff-top or a waterline and visual checking is necessary to evaluate if erosion is associated to bluff-top retreat such as along the Beaufort Sea coast, or due to sediment migration as along barrier islands and spits. Tanguy, Whalen, Prates, Pina, et al. (2023), Tanguy, Whalen, Prates, and Vieira (2023) have shown differences in coastline change rate measurements up to 20% when considering bluff-top/vegetation line or waterline as a shoreline reference. For the purposes of coastal risk assessment along permafrost coasts with the projection of future coastline position, it is necessary to characterize retreat of the bluff-top line rather than migration of dynamic deposition sedimentary features such as beaches, spits and barrier islands.

Due to the noticeable inter-decade variability of coastline changes found at validation sites (Figure 6), which is also confirmed by multiple previous studies (Farquharson et al., 2018; Jones et al., 2018; Tanguy, Whalen, Prates, Pina, et al., 2023; Tanguy, Whalen, Prates, & Vieira, 2023), we can expect a rapid and strong response of permafrost coasts to reduced sea-ice and in consequence increasing storm and wave action, but there likely will nevertheless also be periods of slower rates locally that results in a high shoreline change variability. Sea-ice variability during winter and the length of the open-water season significantly impact coastal erosion along unconsolidated and exposed coasts, such as the Beaufort and Laptev Sea coasts (Günther et al., 2020).

Barnhart et al. (2014) highlights an increase in the open-water season, leading to greater storm exposure. Locally, this results in increasing fetch area, as seen at Drew Point, Alaska, where larger, more energetic waves enhance erosion. Although quantifying this relationship regionally remains challenging, it is crucial for understanding Arctic coastline evolution. Additional factors, such as regional SLR, permafrost temperature, ground-ice content, and thaw subsidence, also contribute to the acceleration of permafrost coastline retreat, particularly along unconsolidated coasts. Integrating these variables and refining time-period analyses are necessary to improve our understanding of coastal erosion drivers.

6.3. Permafrost Thaw

The GT and ALT Permafrost_cci products have been validated with various in-situ measurements. However, the data sets reveal regional biases associated with the spatial resolution (near 1 km) of the modeled data sets, which do not capture land-cover spatial variability at a finer scale. Ground stratigraphy and snow cover are significant controlling factors for ALT. The currently used ground stratigraphies in the Permafrost_cci modeling are derived from land-cover classification (Palmtag et al., 2022; Westermann, Langer, et al., 2015; Westermann, Østby, et al., 2015) and do not consistently represent real ground conditions. Hence, significant errors are expected where bedrock is actually represented as moisture-rich ground. Thus, the characterization of change using relative values is more adapted than the use of absolute values. However, increasing ALT is not always inducing subsidence. Since the study area extends over the Arctic region and considers permafrost-dominated coasts, some areas may show deep active layer thickness where its increasing trend is less relevant for risk assessment. However, permafrost thaw is not linear and uniform and heat transfer depends on surface water conditions. Long-term simulations spanning from 1901 to 2100, which utilize reanalysis data and climate model outputs, reveal that the hydrological regime can accelerate or slow down the thawing of permafrost (Westermann, Langer, et al., 2015; Westermann, Østby, et al., 2015). Increasing ALT might be relevant in areas characterized by shallow ALT, such as higher latitudes Arctic settlements where subsidence and infrastructure instabilities can be caused by an abrupt increase in thaw depth (Nitzbon et al., 2020).

Permafrost temperature trends serve as a critical proxy for assessing regions at risk of thaw subsidence. Along coastal areas, this process can lead to rapid landward coastlines, migration, accelerated flooding, and significant land loss, particularly as this process occurs regionally at rates faster than SLR (Forbes et al., 2022). The experimental study by Wagner et al. (2018) has shown the significant effect of increasing GT with permafrost thaw by deepening of the permafrost table and subsidence. Based on an area of 143 m^2, and 1.5 m soil depth, their results reveal a linear relationship between GT increase and subsidence where an augmentation of 13°C results in ALT increase of 1 m and subsidence of 10 cm. Studies have shown that summer surface subsidence is derivable over low-land permafrost regions from, for example, Sentinel-1 SAR. In the area of Point Lonely Air Field, ground surface displacement ranged between 2 and 6 cm in the summer 2017. However, long time series and in-situ data are lacking to validate the recorded subsidence within the InSAR pixel scale (Strozzi et al., 2018). Assessment of risk areas associated to increasing ALT would need to consider the actual ALT.

Permafrost degradation can intensify thermokarst processes, changing landscapes and significantly impacting Arctic hydrology by accelerating thermo-hydrological erosion (Grosse et al., 2013; Liljedahl et al., 2016; Tanguy, Whalen, Prates, Pina, et al., 2023; Tanguy, Whalen, Prates, & Vieira, 2023). Combined with permafrost degradation, such erosion can further lead to the spread of contaminants in the environment. Toxic substances are naturally present in permafrost terrain and can also be found in buried waste and landfill sites in industrial areas. As permafrost thaws and erosion increases, these contaminants, including heavy metals and persistent organic pollutants, can be released into surrounding ecosystems. These changes pose significant environmental and ecological risks in Arctic regions, impacting water quality, wildlife, and human health (Langer et al., 2023).

6.4. Exposed Infrastructure and Settlements

The combined analysis of the coastline change data set and the SACHI-v2 data set allows the identification of settlements and infrastructure exposed to coastal erosion, from short-to long-term periods (2030, 2050, and 2100) and to SLR in 2100. Note that in this study, the definition of settlement is mainly based on the concentration of infrastructure which are sometimes associated with industrial or military facilities along the coast and where people are not permanently living. It is therefore important to consider this for risk assessment, since arctic

indigenous communities, rely on seasonal hunting and fishing for subsistence. Meanwhile, industries like mining have greater financial resources to adapt to environmental changes, such as permafrost thaw, or to relocate facilities. Indigenous knowledge and their diverse perspectives needs to be integrated in adaptation strategies to climate risks (IPCC, 2023). Note that settlements, which are already exposed to coastal erosion are also included in the results. Examples include Tuktoyaktuk and Newtok, where infrastructure relocalization strategies are planned or taking place. However, in Alaska, some settlements currently under of erosion threat were not identified in our analysis. This is the case for example, for Utqiagvik (Barrow), Kivalina, and other settlements in northwest Alaska (Figure A1). We noticed that some quality issues in the Landsat data from 2003 may have produced artifacts and classification errors in the detected area of change, but also that highly dynamic coastal features such as barrier islands can pose methodical challenges for the detection. In some locations, the results are coherent with local measurements found in the literature, such as in the study of Nicu et al. (2021), who investigated coastline changes and potential impacts at the cultural heritage site of Hiorthhamn in Svalbard (78° 14′50″ N, 15°42′30″ E). Among the 56 coastal settlements in Alaska, our pan-Arctic approach was able to identify 25 settlements being exposed to coastal erosion by 2100. These results agree for 11 settlements, also identified by Buzard et al. (2021), with the identification of 14 additional settlements mostly located along the Beaufort Sea coast. In Greenland, no settlements were found to be directly exposed to coastal erosion, mainly due to the solid rock composition of the majority the coastline, and due to isostatic rebound effect. Moreover, due to the spatial resolution of the Landsat data, our results do not consider changes below 2 m/yr. Therefore, some infrastructure and settlements potentially exposed could have been omitted from our results and local coastline change assessments remain necessary. Although Greenland is considered to have relatively stable and safe coasts, it is actually exposed to extreme wave events from tsunamis triggered by submarine landslides or glacier calving. These factors were not considered in our assessment, but are critical to understand settlement exposure in the region (Kostrzewa et al., 2024; Strzelecki & Jaskólski, 2020; Svennevig et al., 2024).

In addition, regional SLR projection for 2100 along the studied coasts was investigated to identify settlements potentially affected by SLR in 2100, since 60% of coastal infrastructure are located in low-lying areas (<10 m). The Beaufort Sea was identified as a hot-spot for SLR by 2100. However, this result should be taken with caution, as it may be influenced by a single, high subsidence rate recorded at the Prudhoe Bay tide gauge (0.37 m/century). Spatial extrapolation of such limited subsidence data can introduce uncertainty, potentially leading to over-estimated SLR along the Beaufort Sea coast. Although AR6 projections have improved regional accuracy, validation remains challenging in polar regions due to sparse long-term data, making extrapolations of subsidence and SLR more uncertain (Slangen et al., 2023). The use of the DeltaDTM model is deemed suitable for large SLR scenarios. For finer increments (below 1 m), the model's reliability decreases to 50% (Pronk et al., 2024). Various models and frameworks exist that integrate satellite observation, coastal elevation and SLR to determine chronic marine submersion and coastline responses to waves (Terres de Lima et al., 2021; Vitousek et al., 2023), however, the implementation of these models remains challenging at the regional scale, especially in the Arctic region.

Overall, using linear extrapolation to predict future coastline positions is primarily a bench-marking tool. It does not account for numerous external factors that could affect coastline retreat, such as ground-ice content, sea surface temperature, SLR, subsidence, and nearshore sediment dynamics. Quantifying these factors at a circum-Arctic scale remains challenging and should be integrated into predictive models.

For the first time, our data set allows for a pan-Arctic estimation of the number of settlements exposed to current and future coastal erosion, warming permafrost temperature, and active layer thickening. However, the very likely intensification of drivers of coastal erosion, such as more intense storm surges and lengthening of the open-water season, were not incorporated in our analyses. Thus, it is likely that our results present a rather conservative estimation of the total number of coastal settlements being affected by coastal erosion in the future. Infrastructure damage and associated costs within coastal areas needs also to be assessed to quantify economic consequences (Buzard et al., 2021; Jaskólski, 2021; Ogorodov et al., 2023; Streletskiy et al., 2019).

7. Conclusions

Our study has demonstrated the effectiveness of remote sensing techniques in assessing the evolution of Arctic and permafrost coastline across the Arctic over the last 20 years, with a novel workflow to derive rates of change. Change probabilities so far used for inland lake change monitoring have been applied to coastal change and a

geometry-based rate retrieval method was successfully demonstrated, which allows partial automatization. The results show that erosion dominates along coastal settlement areas, with retreat rates of up to 19 m/yr. Extrapolation of the coastline position by the year 2030 revealed that 18% of coastal settlements will be affected by coastal erosion, and 21% in 2100. The majority of identified settlements with exposure are localized along the Alaskan and Siberian coasts. The results in identified exposed settlements are conservative due to the data quality, spatial resolution, and time-span which is influencing the significant erosion detection.

Simultaneously, ground temperature has shown a significant warming trend of 0.8°C per decade and the active layer is deepening by 6 cm per decade over the entire study area. Indeed, nearly 45% of infrastructure are built in areas where ground temperature is rising from 1 to 2°C/decade and 85% above active layer deepening from 0 to 4 cm/decade. Based on these trends, 77% of the coastal infrastructure, will experience a shift to positive ground temperatures by 2100. These results indicate a potential vulnerability of unconsolidated coastal permafrost to ground subsidence, flooding hazards, and changes in hydrological systems.

With 60% of the coastal infrastructure located in low-lying areas, SLR is expected to affect 45% of the coastal settlements by 2100. In combination with the effects cited above, the vulnerability of Arctic and permafrost coastal settlements is increasing. Although minimal changes and exposure have been identified along high Arctic coasts like Greenland, it's crucial to recognize the unique coastal hazards of this region, where populations must cope with the risk of tsunamis. Additionally, glacier calving and the destabilization of mountain slopes present new challenges for communities in this area. To minimize the risks and costs faced by coastal permafrost settlements, rapid adoption of coastline management and adaptation measures is essential to protect infrastructure and the livelihoods of local populations.

In the context of changing permafrost conditions, this work provides relevant information at the pan-Arctic scale for the identification of coastal settlements at risk by several time steps until the end of the 21st century. This is an important first step toward a remote sensing-based pan-Arctic monitoring system and developing mitigation strategies, thus reducing the vulnerability of Arctic settlements to future coastal hazards.

Appendix A

Figure A1. Example of rapid coastal erosion threatening coastal infrastructures at Utqiagvik (Barrow, Alaska). The photo was taken in September 2024. A road portion was destroyed after a storm during the summer 2023, we note the presence of red tanks and remaining big-bags down the bluff. Image credit: Benjamin Jones.
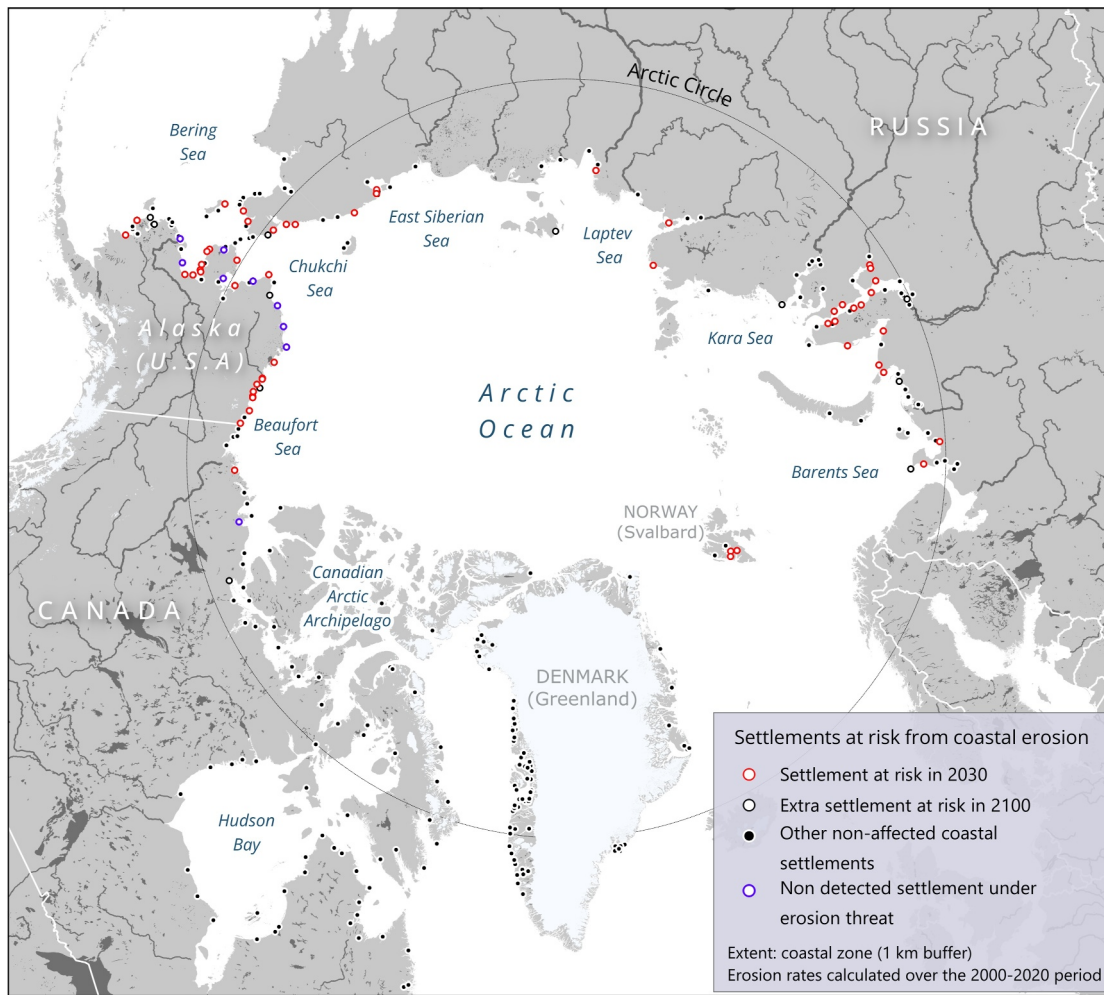
Figure A2. Settlements potentially exposed to coastal erosion from 2030 to 2100. Contains modified Copernicus Sentinel data 2016 to 2022. Background: GSHHG (Wessel & Smith, 1996).
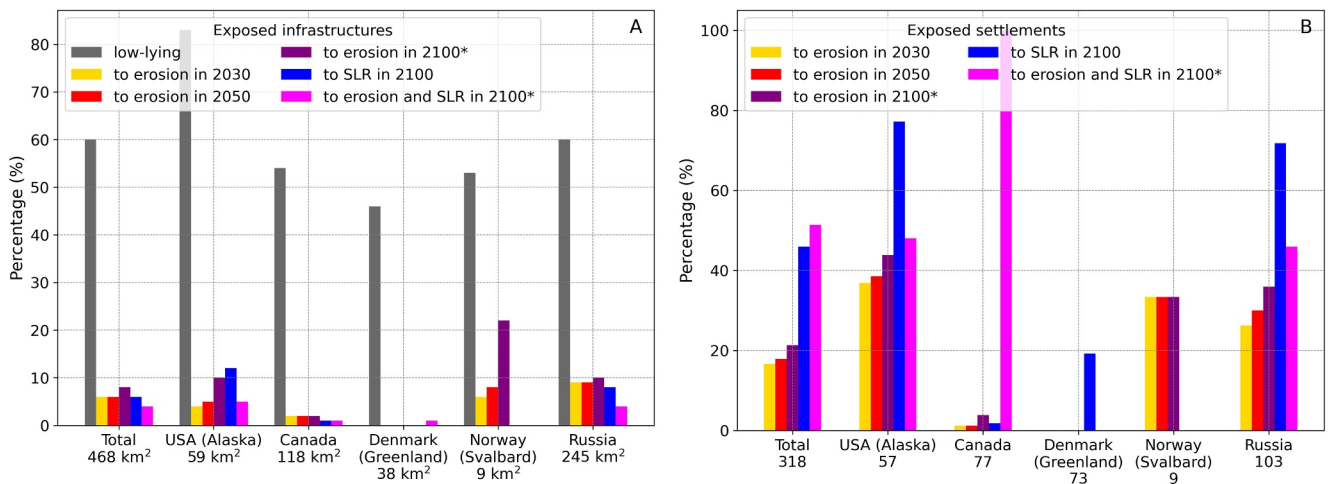

Figure A3. Percentages of infrastructures (a) and settlements (b) exposed to erosion and Sea-Level Rise (SLR). Total area (km^2) and settlement count are below country names. In panel (a), the percentages are calculated relatively to the low-lying coastal infrastructures area and in panel (b) to the total coastal settlements. *combined exposition from erosion and SLR category (pink bar) is relative to the total exposed features to erosion in 2100.

Disclaimer

This study and associated data sets were designed for scientific purposes only and should not be taken as professional engineering advice.

Data Availability Statement

This study is based on the SACHI-v2 infrastructure data set published from Bartsch et al. (2024), available in Zenodo repository: https://doi.org/10.5281/zenodo.10160636. Time series for permafrost active layer thickness is available from Obu et al. (2021a) in CEDA: https://doi.org/10.5285/67a3f8c8dc914ef99f7f08eb0d997e23. Time series for permafrost ground temperature is available from Obu et al. (2021b) in CEDA: https://doi.org/10.5285/b25d4a6174de4ac78000d034f500a268. We used the digital terrain model DeltaDTM from Pronk et al. (2024) available at: https://doi.org/10.4121/21997565.v2. Regional SLR projection from Garner et al. (2022) in Zenodo: https://doi.org/10.5281/zenodo.6382554. Permafrost active layer thickness validation was based on in-situ measurements from Streletskiy and Shiklomanov (2021) (https://arcticdata.io/catalog), Martin et al. (2023) (https://doi.pangaea.de/10.1594/PANGAEA.956039) and CALM et al. (2024). Additional published data used for validation are available in Solomon (2005), Ehrich et al. (2019), Gibbs et al. (2020), Ingeman-Nielsen and Vakulenko (2018), Lu et al. (2018), (https://www.sciencebase.gov/catalog/item/5fa1f10ad34e198cb793cee4; https://doi.org/10.1594/PANGAEA.895949; https://doi.org/10.1594/PANGAEA.895950). These data sets are described in the Supporting Information file. The data produced by this work is available in Zenodo (settlements and attributes, Tanguy et al., 2024).

References

Andrews, J. T. (1970). Present and postglacial rates of uplift for glaciated northern and eastern North America derived from postglacial uplift curves. *Canadian Journal of Earth Sciences*, 7(2), 703–715. https://doi.org/10.1139/e70-06

Atkinson, D. E. (2005). Observed storminess patterns and trends in the circum-Arctic coastal regime. *Geo-Marine Letters*, 25(2–3), 98–109. https://doi.org/10.1007/s00367-004-0191-0

Barnhart, K., Overeem, I., & Anderson, R. (2014). The effect of changing sea ice on the physical vulnerability of arctic coasts. *The Cryosphere*, 8(5), 1777–1799. https://doi.org/10.5194/tc-8-1777-2014

Bartsch, A., Ley, S., Nitze, I., Pointner, G., & Vieira, G. (2020). Feasibility study for the application of synthetic aperture radar for coastal erosion rate quantification across the arctic. *Frontiers in Environmental Science*, 8, 143. https://doi.org/10.3389/fenvs.2020.00143

Bartsch, A., Pointner, G., Ingeman-Nielsen, T., & Lu, W. (2020). Towards circumpolar mapping of arctic settlements and infrastructure based on Sentinel-1 and Sentinel-2. *Remote Sensing*, 12(15), 2368. https://doi.org/10.3390/rs12152368

Bartsch, A., Pointner, G., Nitze, I., Efimova, A., Jakober, D., Ley, S., et al. (2021). Expanding infrastructure and growing anthropogenic impacts along Arctic coasts. *Environmental Research Letters*, 16(11), 115013. https://doi.org/10.1088/1748-9326/ac3176

Bartsch, A., Strozzi, T., & Nitze, I. (2023). Permafrost monitoring from space. *Surveys in Geophysics*, 44(5), 1579–1613. https://doi.org/10.1007/s10712-023-09770-3

Bartsch, A., Widhalm, B., von Baeckmann, C., Efimova, A., Tanguy, R., & Pointner, G. (2024). Sentinel-1/2 derived arctic coastal human impact dataset (SACHI) (v2.0) [Dataset]. *Zenodo*. https://doi.org/10.5281/zenodo.10160636

Bergstedt, H., Zwieback, S., Bartsch, A., & Leibman, M. (2018). Dependence of c-band backscatter on ground temperature, air temperature and snow depth in arctic permafrost regions. *Remote Sensing*, 10(1), 142. https://doi.org/10.3390/rs10010142

Biskaborn, B. K., Smith, S. L., Noetzli, J., Matthes, H., Vieira, G., Streletskiy, D. A., et al. (2019). Permafrost is warming at a global scale. *Nature Communications*, 10(1), 264. https://doi.org/10.1038/s41467-018-08240-4

Boike, J., Chadburn, S., Martin, J., Zwieback, S., Althuizen, I. H., Anselm, N., et al. (2021). Standardized monitoring of permafrost thaw: A user-friendly, multiparameter protocol. *Arctic Science*, 8(1), 153–182. https://doi.org/10.1139/as-2021-0007

Boisson, A., & Allard, M. (2020). Morphological and evolutionary patterns of emerging arctic coastal landscapes: The case of northwestern Nunavik (Quebec, Canada). *Arctic Science*, 6(4), 488–508. https://doi.org/10.1139/as-2020-0002

Buzard, R., Turner, M., Miller, K., Antrobus, D., & Overbeck, J. (2021). *Erosion exposure assessment of infrastructure in Alaska coastal communities* (Tech. Rep. No. RI 2021-3). Alaska Division of Geological & Geophysical Surveys. https://doi.org/10.14509/30672

CALM, GTN-P, Wieczorek, M., Heim, B., & Bartsch, A. (2024). GTN-P CALM: 34 years of Active Layer Thickness (ALT) across latitudinal and elevational gradients in the Northern Hemisphere [Dataset]. *PANGAEA*. https://doi.pangaea.de/10.1594/PANGAEA.972777

Cazenave, A., Meyssignac, B., Ablain, M., Balmaseda, M., Bamber, J., Barletta, V., et al. (2018). Global sea-level budget 1993–present. *Earth System Science Data*, 10(3), 1551–1590. https://doi.org/10.5194/essd-10-1551-2018

Cooper, J. A. G., & Pilkey, O. H. (2004). Sea-Level rise and shoreline retreat: Time to abandon the Bruun Rule. *Global and Planetary Change*, 43(3–4), 157–171. https://doi.org/10.1016/j.gloplacha.2004.07.001

Crawford, A., Lukovich, J. V., McCrystall, M. R., Stroeve, J. C., & Barber, D. G. (2022). Reduced sea ice enhances intensification of winter storms over the Arctic Ocean. *Journal of Climate*, 35(11), 3353–3370. https://doi.org/10.1175/JCLI-D-21-0747.1

Crawford, A., Stroeve, J., Smith, A., & Jahn, A. (2021). Arctic open-water periods are projected to lengthen dramatically by 2100. *Communications Earth & Environment*, 2(1), 109. https://doi.org/10.1038/s43247-021-00183-x

Cunliffe, A. M., Tanski, G., Radosavljevic, B., Palmer, W. F., Sachs, T., Lantuit, H., et al. (2019). Rapid retreat of permafrost coastline observed with aerial drone photogrammetry. *The Cryosphere*, 13(5), 1513–1528. https://doi.org/10.5194/tc-13-1513-2019

Day, J. J., & Hodges, K. I. (2018). Growing land-sea temperature contrast and the intensification of arctic cyclones. *Geophysical Research Letters*, 45(8), 3673–3681. https://doi.org/10.1029/2018GL077587

Del Río, L., & Gracia, F. (2013). Error determination in the photogrammetric assessment of shoreline changes. *Natural Hazards*, 65(3), 2385–2397. https://doi.org/10.1007/s11069-012-0407-y

Ehrich, D., Thuestad, A. E., Tømmervik, H., Fauchald, P., & Hausner, V. H. (2019). Local land use associated with socio-economic development in six arctic regions. *Ambio*, *48*(6), 649–660. https://doi.org/10.1007/s13280-018-1095-y

ESA. (2023). Copernicus DEM - Global and European digital elevation model (COP-DEM) [Dataset]. https://doi.org/10.5270/ESA-c5d3d65

Farquharson, L., Mann, D., Swanson, D., Jones, B., Buzard, R., & Jordan, J. (2018). Temporal and spatial variability in coastline response to declining sea-ice in northwest Alaska. *Marine Geology*, *404*, 71–83. https://doi.org/10.1016/J.MARGEO.2018.07.007

Forbes, D. L., Craymer, M., James, T., & Whalen, D. (2022). Subsidence drives habitat loss in a large permafrost delta, Mackenzie river outlet to the Beaufort Sea, western arctic Canada. *Canadian Journal of Earth Sciences*, *59*(11), 914–934. https://doi.org/10.1139/cjes-2021-0127

Fox-Kemper, B., Hewitt, H. T., Xiao, C., Aðalgeirsdóttir, G., Drijfhout, S. S., Edwards, T. L., et al. (2021). Ocean, cryosphere and sea level change. In V. Masson-Delmotte, P. Zhai, A. Pirani, S. L. Connors, C. Péan, S. Berger, et al. (Eds.), *Climate change 2021: The physical science basis. Contribution of working group 1 to the sixth assessment report of the Intergovernmental Panel on Climate Change* (pp. 1211–1362). Cambridge University Press. https://doi.org/10.1017/9781009157896.011

Frederikse, T., Landerer, F., Caron, L., Adhikari, S., Parkes, D., Humphrey, V. W., et al. (2020). The causes of sea-level rise since 1900. *Nature*, *584*(7821), 393–397. https://doi.org/10.1038/s41586-020-2591-3

Garner, G. G., Hermans, T., Kopp, R. E., Slangen, A. B. A., Edwards, T. L., Levermann, A., et al. (2022). IPCC AR6 sea level projections [Dataset]. *Zenodo*. https://doi.org/10.5281/zenodo.6382554

Gibbs, A., Erikson, L. H., Jones, B. M., Richmond, B. M., & Engelstad, A. C. (2021). Seven decades of coastal change at Barter Island, Alaska: Exploring the importance of waves and temperature on erosion of coastal permafrost bluffs. *Remote Sensing*, *13*(21), 4420. https://doi.org/10.3390/rs13214420

Gibbs, A., Jones, B., & Richmond, B. (2020). A GIS compilation of vector shorelines and coastal bluff edge positions, and associated rate-of-change data for Barter Island, Alaska [Dataset]. *USGS, Pacific Coastal and Marine Science Center*. https://doi.org/10.5066/P9CRBC5I

Glotov, V. E., Chlachula, J., Glotova, L. P., & Little, E. (2018). Causes and environmental impact of the gold-tailings dam failure at Karamken, the Russian far east. *Engineering Geology*, *245*, 236–247. https://doi.org/10.1016/j.enggeo.2018.08.012

Grosse, G., Jones, B. M., & Arp, C. D. (2013). Thermokarst lakes, drainage, and drained basins. *Treatise on Geomorphology*, *8*, 325–353. https://doi.org/10.1016/B978-0-12-374739-6.00216-5

Günther, F., Overduin, P., Sandakov, A., Grosse, G., & Grigoriev, M. (2020). Coastal erosion variability at the southern Laptev sea linked to winter sea ice and the arctic oscillation. *Geophysical Research Letters*, *47*(3), e2019GL086876. https://doi.org/10.1029/2019GL086876

Guo, D., Wang, H., Romanovsky, V., Haywood, A., Pepin, N., Salzmann, U., et al. (2023). Highly restricted near-surface permafrost extent during the mid-Pliocene warm period. *Proceedings of the National Academy of Sciences of the United States of America*, *120*(36), e2301954120. https://doi.org/10.1073/pnas.2301954120

Hansen, H. O., Nordstrom, M., Winkelmann, D., & Lantuit, H. (2015). Acceleration of coastal-retreat rates for high-arctic rock cliffs on Brøggerhalvøya, Svalbard, over the past decade. *Geology*, *43*(11), 1031–1034. https://doi.org/10.5194/esurf-12-1049-2024

Heim, B., Lisovski, S., Wieczorek, M., Pellet, C., Delaloye, R., Bartsch, A., et al. (2021). *D4.1 products validation and intercomparision report (pvir)* (Tech. Rep.). European Space Agency. https://climate.esa.int/media/documents/CCI_PERMA_PVIR_v3.0_20210930.pdf

Henke, M., Miesse, T., de Lima, A. D. S., Ferreira, C. M., & Ravens, T. M. (2024). Increasing coastal exposure to extreme wave events in the Alaskan arctic as the open water season expands. *Communications Earth & Environment*, *5*(1), 165. https://doi.org/10.1038/s43247-024-01323-9

Hjort, J., Streletskiy, D., Doré, G., Wu, Q., Bjella, K., & Luoto, M. (2022). Impacts of permafrost degradation on infrastructure. *Nature Reviews Earth & Environment*, *3*(1), 24–38. https://doi.org/10.1038/s43017-021-00247-8

Ingeman-Nielsen, T., & Vakulenko, I. (2018). Calibration and validation data for infratructure mapping, Greenland [Dataset]. *PANGAEA*. https://doi.org/10.1594/PANGAEA.895949

IPCC. (2023). Ocean, cryosphere and sea level change. In *Climate change 2021 – the physical science basis: Working group i contribution to the sixth assessment report of the intergovernmental panel on climate change* (pp. 1211–1362). Cambridge University Press. https://doi.org/10.1017/9781009157896.011

Irrgang, A. M., Bendixen, M., Farquharson, L. M., Baranskaya, A. V., Erikson, L. H., Gibbs, A. E., et al. (2022). Drivers, dynamics and impacts of changing Arctic coasts. *Nature Reviews Earth & Environment*, *3*(1), 39–54. https://doi.org/10.1038/s43017-021-00232-1

Irrgang, A. M., Lantuit, H., Gordon, R. R., Piskor, A., & Manson, G. K. (2019). Impacts of past and future coastal changes on the Yukon Coast—Threats for cultural sites, infrastructure, and travel routes. *Arctic Science*, *5*(2), 107–126. https://doi.org/10.1139/as-2017-0041

Irrgang, A. M., Lantuit, H., Manson, G. K., Günther, F., Grosse, G., & Overduin, P. P. (2018). Variability in rates of coastal change along the Yukon Coast, 1951 to 2015. *Journal of Geophysical Research: Earth Surface*, *123*(4), 779–800. https://doi.org/10.1002/2017JF004326

Isaev, V., Koshurnikov, A., Pogorelov, A., Amangurov, R., Podchasov, O., Sergeev, D., et al. (2019). Cliff retreat of permafrost coast in southwest Baydaratskaya Bay, Kara Sea, during 2005–2016. *Permafrost and Periglacial Processes*, *30*(1), 35–47. https://doi.org/10.1002/ppp.1993

Jaskólski, M. W. (2021). For human activity in Arctic coastal environments–a review of selected interactions and problems. *Miscellanea Geographica*, *25*(2), 127–143. https://doi.org/10.2478/mgrsd-2020-0036

Jaskólski, M. W., Pawłowski, Ł., & Strzelecki, M. C. (2018). High arctic coasts at risk—The case study of coastal zone development and degradation associated with climate changes and multidirectional human impacts in Longyearbyen (Adventfjorden, Svalbard). *Land Degradation & Development*, *29*(8), 2514–2524. https://doi.org/10.1002/ldr.2974

Jin, Y., Chen, M., Yan, H., Wang, T., & Yang, J. (2023). Sea level variation in the Arctic Ocean since 1979 based on ORAS5 data. *Frontiers in Marine Science*, *10*, 1197456. https://doi.org/10.3389/fmars.2023.1197456

Jones, B., Farquharson, L., Baughman, C. A., Buzard, R., Arp, C., Grosse, G., et al. (2018). A decade of remotely sensed observations highlight complex processes linked to coastal permafrost bluff erosion in the Arctic. *Environmental Research Letters*, *13*(11), 115001. https://doi.org/10.1088/1748-9326/aae471

Jorgenson, M. T., Shur, Y., & Pullman, E. R. (2008). Permafrost characteristics of Alaska - 2008 Shapefile [Dataset]. *U.S. Geological Survey (USGS)*. https://catalog.data.gov/dataset/permafrost-characteristics-of-alaska-2008

Kopp, R. E., Garner, G. G., Hermans, T. H. J., Jha, S., Kumar, P., Reedy, A., et al. (2023). The Framework for Assessing Changes to Sea-Level (FACTS) v1.0: A platform for characterizing parametric and structural uncertainty in future global, relative, and extreme sea-level change. *Geoscientific Model Development*. *16*, 7461–7489. https://doi.org/10.5194/gmd-16-7461-2023

Kostrzewa, O., Szczypińska, M., Kavan, J., Senderak, K., Novák, M., & Strzelecki, M. C. (2024). A boulder beach formed by waves from a calving glacier revisited: Multidecadal tsunami–controlled coastal changes in front of Eqip Sermia, west Greenland. *Permafrost and Periglacial Processes*, *35*(3), 312–325. https://doi.org/10.1002/ppp.2235

Kumar, D. (2021). Urban objects detection from c-band synthetic aperture radar (SAR) satellite images through simulating filter properties. *Scientific Reports*, *11*(1), 6241. https://doi.org/10.1038/s41598-021-85121-9

Kurtze, D. A. (2022). Gravitational effects of ice sheets on sea level. *American Journal of Physics*, *90*(5), 351–358. https://doi.org/10.1119/5.0067924

Langer, M., von Deimling, T. S., Westermann, S., Rolph, R., Rutte, R., Antonova, S., et al. (2023). Thawing permafrost poses environmental threat to thousands of sites with legacy industrial contamination. *Nature Communications*, *14*(1), 1721. https://doi.org/10.1038/s41467-023-37276-4

Lantuit, H., Overduin, P. P., Couture, N., Wetterich, S., Aré, F., Atkinson, D., et al. (2012). The arctic coastal dynamics database: A new classification scheme and statistics on arctic permafrost coastlines. *Estuaries and Coasts*, *35*(2), 383–400. https://doi.org/10.1007/s12237-010-9362-6

Liljedahl, A. K., Boike, J., Daanen, R. P., Fedorov, A. N., Frost, G. V., Grosse, G., et al. (2016). Pan-Arctic ice-wedge degradation in warming permafrost and its influence on tundra hydrology. *Nature Geoscience*, *9*(4), 312–318. https://doi.org/10.1038/ngeo2674

Lu, W., Aalberg, A., Høyland, K., Lubbad, R., Løset, S., & Ingeman-Nielsen, T. (2018). Calibration data for infratucture mapping in Svalbard, link to files [Dataset]. https://doi.org/10.1594/PANGAEA.895950

Malenfant, F., Whalen, D., Fraser, P., & van Proosdij, D. (2022). Rapid coastal erosion of ice-bonded deposits on Pelly Island, southeastern Beaufort sea, Inuvialuit settlement region, western Canadian arctic. *Canadian Journal of Earth Sciences*, *59*(11), 961–972. https://doi.org/10.1139/cjes-2021-0118

Marino, E., & Lazrus, H. (2015). Migration or forced displacement? The complex choices of climate change and disaster migrants in Shishmaref, Alaska and Nanumea, Tuvalu. *Human Organization*, *74*(4), 341–350. https://doi.org/10.17730/0018-7259-74.4.341

Martin, J., Boike, J., Chadburn, S., Zwieback, S., Anselm, N., Goldau, M., et al. (2023). T-MOSAiC 2021 myThaw data set [Dataset]. *PANGAEA*. https://doi.org/10.1594/PANGAEA.956039

Masson-Delmotte, V., Zhai, P., Pirani, A., Connors, S. L., Péan, C., Berger, S., et al. (2021). *Climate change 2021: The physical science basis. Contribution of working group I to the sixth assessment report of the intergovernmental panel on climate change*. Cambridge University Press. (Chapter 9: Ocean, Cryosphere and Sea Level Change). https://doi.org/10.1017/9781009157896

Meredith, M., Sommerkorn, M., Cassotta, S., Derksen, C., Ekaykin, A., Hollowed, A., et al. (2019). *Polar regions. Chapter 3, IPCC special report on the ocean and cryosphere in a changing climate* (Tech. Rep.). Intergovernmental Panel on Climate Change.

Miner, K. R., Turetsky, M. R., Malina, E., Bartsch, A., Tamminen, J., McGuire, A. D., et al. (2022). Permafrost carbon emissions in a changing Arctic. *Nature Reviews Earth & Environment*, *3*(1), 55–67. https://doi.org/10.1038/s43017-021-00230-3

Nicu, I. C., Rubensdotter, L., Stalsberg, K., & Nau, E. (2021). Coastal erosion of arctic cultural heritage in danger: A case study from Svalbard, Norway. *Water*, *13*(6), 784. https://doi.org/10.3390/w13060784

Nielsen, D. M., Pieper, P., Barkhordarian, A., Overduin, P., Ilyina, T., Brovkin, V., et al. (2022). Increase in arctic coastal erosion and its sensitivity to warming in the twenty-first century. *Nature Climate Change*, *12*(3), 263–270. https://doi.org/10.1038/s41558-022-01281-0

Nitzbon, J., Schneider von Deimling, T., Aliyeva, M., Chadburn, S. E., Grosse, G., Laboor, S., et al. (2024). No respite from permafrost-thaw impacts in the absence of a global tipping point. *Nature Climate Change*, 1–13. https://doi.org/10.1038/s41558-024-02011-4

Nitzbon, J., Westermann, S., Langer, M., Martin, L. C., Strauss, J., Laboor, S., & Boike, J. (2020). Fast response of cold ice-rich permafrost in northeast Siberia to a warming climate. *Nature Communications*, *11*(1), 2201. https://doi.org/10.1038/s41467-020-15725-8

Nitze, I., Grosse, G., Jones, B. M., Arp, C. D., Ulrich, M., Fedorov, A., & Veremeeva, A. (2017). Landsat-based trend analysis of lake dynamics across northern permafrost regions. *Remote Sensing*, *9*(7), 640. https://doi.org/10.3390/rs9070640

Obu, J., Lantuit, H., Grosse, G., Günther, F., Sachs, T., Helm, V., & Fritz, M. (2017). Coastal erosion and mass wasting along the Canadian Beaufort Sea based on annual airborne lidar elevation data. *Geomorphology*, *293*, 331–346. https://doi.org/10.1016/j.geomorph.2016.02.014

Obu, J., Westermann, S., Barboux, C., Bartsch, A., Delaloye, R., Grosse, G., et al. (2021c). Permafrost extent for the northern hemisphere, v3.0., centre for environmental data analysis [Dataset]. https://doi.org/10.5285/6e2091cb0c8b4106921b63cd5357c97c

Obu, J., Westermann, S., Barboux, C., Bartsch, A., Delaloye, R., Grosse, G., et al. (2021a). ESA permafrost climate change initiative (Permafrost_cci): Permafrost active layer thickness for the northern hemisphere, v3.0 [Dataset]. *NERC EDS Centre for Environmental Data Analysis*. https://doi.org/10.5285/67a3f8c8dc914ef99f7f08eb0d997e23

Obu, J., Westermann, S., Barboux, C., Bartsch, A., Delaloye, R., Grosse, G., et al. (2021b). ESA permafrost climate change initiative (Permafrost_cci): Permafrost ground temperature for the northern hemisphere, v3.0 [Dataset]. *NERC EDS Centre for Environmental Data Analysis*. https://doi.org/10.5285/b25d4a6174de4ac78000d034f500a268

Ogorodov, S., Aleksyutina, D., Baranskaya, A., Shabanova, N., & Shilova, O. (2020). Coastal erosion of the Russian arctic: An overview. *Journal of Coastal Research*, *95*(SI), 599–604. https://doi.org/10.2112/SI95-117.1

Ogorodov, S., Badina, S., & Bogatova, D. (2023). Sea coast of the western part o the Russian arctic under climate change: Dynamics, technogenic influence and potential economic damage. *Climate*, *11*(7), 143. https://doi.org/10.3390/cli11070143

Overduin, P. P., Strzelecki, M. C., Grigoriev, M. N., Couture, N., Lantuit, H., St-Hilaire-Gravel, D., et al. (2014). Coastal changes in the arctic. *Geological Society, London, Special Publications*, *388*(1), 103–129. https://doi.org/10.1144/SP388.13

Overeem, I., Anderson, R. S., Wobus, C. W., Clow, G. D., Urban, F. E., & Matell, N. (2011). Sea ice loss enhances wave action at the arctic coast. *Geophysical Research Letters*, *38*(17). https://doi.org/10.1029/2011GL048681

Palmtag, J., Obu, J., Kuhry, P., Richter, A., Siewert, M. B., Weiss, N., et al. (2022). A high spatial resolution soil carbon and nitrogen dataset for the northern permafrost region based on circumpolar land cover upscaling. *Earth System Science Data*, *14*(9), 4095–4110. https://doi.org/10.5194/essd-14-4095-2022

Pronk, M. (2024). Deltadtm: A global coastal digital terrain model [Dataset]. *ResearchData*. https://doi.org/10.4121/21997565.V2.4TU

Pronk, M., Hooijer, A., Eilander, D., Haag, A., de Jong, T., Vousdoukas, M., et al. (2024). Deltadtm: A global coastal digital terrain model. *Scientific Data*, *11*(1), 273. https://doi.org/10.1038/s41597-024-03091-9

Ramage, J., Jungsberg, L., Wang, S., Westermann, S., Lantuit, H., & Heleniak, T. (2021). Population living on permafrost in the arctic. *Population and Environment*, *43*, 1–17. https://doi.org/10.1007/s11111-020-00370-6

Robertson, L. (2015). Surficial geology index map [Dataset]. *Geological Survey of Canada*. https://open.canada.ca/data/en/dataset/cebc283f-bae1-4eae-a91f-a26480cd4e4a

Slangen, A. B., Palmer, M. D., Camargo, C. M., Church, J. A., Edwards, T. L., Hermans, T. H., et al. (2023). The evolution of 21st century sea-level projections from IPCC AR5 to AR6 and beyond. *Cambridge Prisms: Coastal Futures*, *1*, e7. https://doi.org/10.1017/cft.2022.8

Smith, S. L., O'Neill, H. B., Isaksen, K., Noetzli, J., & Romanovsky, V. E. (2022). The changing thermal state of permafrost. *Nature Reviews Earth & Environment*, *3*(1), 10–23. https://doi.org/10.1038/s43017-021-00240-1

Solomon, S. M. (2005). Spatial and temporal variability of shoreline change in the Beaufort-Mackenzie region, northwest territories, Canada. *Geo-Marine Letters*, *25*(2–3), 127–137. https://doi.org/10.1007/s00367-004-0194-x

Streletskiy, D., & Shiklomanov, N. (2021). Circum polar active layer monitoring (calm) [Dataset]. *Arctic Data Center*. https://arcticdata.io/catalog

Streletskiy, D. A., Suter, L., Shiklomanov, N. I., Porfiriev, B. N., & Eliseev, D. O. (2019). Assessment of climate change impacts on buildings, structures and infrastructure in the Russian regions on permafrost. *Environmental Research Letters*, *14*(2), 025003. https://doi.org/10.1088/1748-9326/aaf5e6

Stolbovoi, V., & McCallum, I. (2002). Land resources of Russia—Soils (Russian National classification) [Dataset]. *International Institute for Applied Systems Analysis and the Russian Academy of Science*. Retrieved from https://databasin.org/datasets/cda72e8519994afe9364371413adc50f/

Stroeve, J., & Notz, D. (2018). Changing state of arctic sea ice across all seasons. *Environmental Research Letters*, *13*(10), 103001. https://doi.org/10.1088/1748-9326/aade56

Strozzi, T., Antonova, S., Günther, F., Mätzler, E., Vieira, G., Wegmüller, U., et al. (2018). Sentinel-1 SAR interferometry for surface deformation monitoring in low-land permafrost areas. *Remote Sensing*, *10*(9), 1360. https://doi.org/10.3390/rs10091360

Strzelecki, M. C., & Jaskólski, M. W. (2020). Arctic tsunamis threaten coastal landscapes and communities–survey of Karrat Isfjord 2017 tsunami effects in Nuugaatsiaq, western Greenland. *Natural Hazards and Earth System Sciences*, *20*(9), 2521–2534. https://doi.org/10.5194/nhess-20-2521-2020

Svennevig, K., Hicks, S. P., Forbriger, T., Lecocq, T., Widmer-Schnidrig, R., Mangeney, A., et al. (2024). A rockslide-generated tsunami in a Greenland fjord rang earth for 9 days. *Science*, *385*(6714), 1196–1205. https://doi.org/10.1126/science.adm9247

Tajouri, S., Llovel, W., Sevellec, F., Molines, J.-M., Mathiot, P., Penduff, T., & Leroux, S. (2024). Simulated impact of time-varying river runoff and Greenland freshwater discharge on sea level variability in the Beaufort gyre over 2005–2018. *Journal of Geophysical Research: Oceans*, *129*(9), e2024JC021237. https://doi.org/10.1029/2024JC021237

Tanguy, R., Bartsch, A., Widhalm, B., von Baeckmann, C., Irrgang, A. M., Nitze, I., et al. (2024). Pan-Arctic Coastal Settlements and Infrastructure Vulnerable to Coastal Erosion, Sea-Level Rise, and Permafrost Thaw (1.0) [Dataset]. *Zenodo*. https://doi.org/10.5281/zenodo.14229647

Tanguy, R., Whalen, D., Prates, G., Pina, P., Freitas, P., Bergstedt, H., & Vieira, G. (2023). Permafrost degradation in the ice-wedge tundra terrace of Paulatuk Peninsula (Darnley Bay, Canada). *Geomorphology*, *435*, 108754. https://doi.org/10.1016/j.geomorph.2023.108754

Tanguy, R., Whalen, D., Prates, G., & Vieira, G. (2023). Shoreline change rates and land to sea sediment and soil organic carbon transfer in eastern Parry Peninsula from 1965 to 2020 (Amundsen Gulf, Canada). *Arctic Science*, *9*(3), 506–525. https://doi.org/10.1139/as-2022-0028

Terres de Lima, L., Fernández-Fernández, S., Gonçalves, J. F., Magalhães Filho, L., & Bernardes, C. (2021). Development of tools for coastal management in google earth engine: Uncertainty bathtub model and Bruun rule. *Remote Sensing*, *13*(8), 1424. https://doi.org/10.3390/rs13081424

Thieler, R., Himmelstoss, E., Zichichi, J., & Ergul, A. (2009). *The digital shoreline analysis system (DSAS) version 4.0-an Arcgis extension for calculating shoreline change* (Tech. Rep.). US Geological Survey. https://doi.org/10.3133/ofr20081278

Thomas, M. A., Mota, A., Jones, B. M., Choens, R. C., Frederick, J. M., & Bull, D. L. (2020). Geometric and material variability influences stress states relevant to coastal permafrost bluff failure. *Frontiers in Earth Science*, *8*, 143. https://doi.org/10.3389/feart.2020.00143

Vasiliev, A. A., Drozdov, D. S., Gravis, A. G., Malkova, G. V., Nyland, K. E., & Streletskiy, D. A. (2020). Permafrost degradation in the western Russian arctic. *Environmental Research Letters*, *15*(4), 045001. https://doi.org/10.1088/1748-9326/ab6f12

Vitousek, S., Vos, K., Splinter, K. D., Erikson, L., & Barnard, P. L. (2023). A model integrating satellite-derived shoreline observations for predicting fine-scale shoreline response to waves and sea-level rise across large coastal regions. *Journal of Geophysical Research: Earth Surface*, *128*(7), e2022JF006936. https://doi.org/10.1029/2022JF006936

Wagner, A. M., Lindsey, N. J., Dou, S., Gelvin, A., Saari, S., Williams, C., et al. (2018). Permafrost degradation and subsidence observations during a controlled warming experiment. *Scientific Reports*, *8*(1), 10908. https://doi.org/10.1038/s41598-018-29292-y

Wang, F., Tokarska, K., Zhang, J., Ge, Q., Hao, Z., Zhang, X., & Wu, M. (2018). Climate warming in response to emission reductions consistent with the Paris agreement. *Advances in Meteorology*, *2018*, 1–9. https://doi.org/10.1155/2018/2487962

Wessel, P., & Smith, W. H. (1996). A global, self-consistent, hierarchical, high-resolution shoreline database [Dataset]. *Wiley Online Library*, *101*(B4), 8741–8743. https://doi.org/10.1029/96JB00104

Westermann, S., Langer, M., Boike, J., Heikenfeld, M., Peter, M., Eddon, B., & Krinner, G. (2015). Simulating the thermal regime and thaw processes of ice-rich permafrost ground with the land-surface model Cryogrid 3. *Geoscientific Model Development*, *9*(2), 523–546. https://doi.org/10.5194/GMD-9-523-2016

Westermann, S., Østby, T., Gisnås, K., Schuler, T., & Etzelmüller, B. (2015). A ground temperature map of the north Atlantic permafrost region based on remote sensing and reanalysis data. *The Cryosphere*, *9*(3), 1303–1319. https://doi.org/10.5194/tc-9-1303-2015

Whalen, D., Forbes, D., Kostylev, V., Lim, M., Fraser, P., Nedimović, M., & Stuckey, S. (2022). Mechanisms, volumetric assessment, and prognosis for rapid coastal erosion of Tuktoyaktuk island, an important natural barrier for the Harbour and community. *Canadian Journal of Earth Sciences*, *59*(11), 945–960. https://doi.org/10.1139/cjes-2021-0101

Xu, N. (2018). Detecting coastline change with all available Landsat data over 1986–2015: A case study for the state of Texas, USA. *Atmosphere*, *9*(3), 107. https://doi.org/10.3390/atmos9030107

Zhang, X., Tang, H., Zhang, J., Walsh, J. E., Roesler, E. L., Hillman, B., et al. (2023). Arctic cyclones have become more intense and longer-lived over the past seven decades. *Communications Earth & Environment*, *4*(1), 348. https://doi.org/10.1038/s43247-023-01003-0